Volume 1 | Number 1 | Jan 2013 | Pages 1–100

Journal of
Materials Chemistry A

Materials for energy and sustainability
www.rsc.org/materialsA

ROYAL SOCIETY
OF CHEMISTRY

ROYAL SOCIETY
OF CHEMISTRY

www.rsc.org/materialsA

FEATURE ARTICLE

Recent progress on carbon-based support materials for electrocatalysts of direct methanol fuel cells†

Huajie Huang and Xin Wang*

With the continuously increasing demand of energy along with depletion of conventional fossil fuel reserves and the rapidly escalating environmental problems, direct methanol fuel cells (DMFCs) as alternative green and sustainable power sources have aroused tremendous research interest in academic and engineering circles. In order to achieve high power density as well as low production cost of DMFCs, 10 the well- designed and fabricated anode catalysts with controllable composition, architecture and morphology have been regarded as a key point for realizing high-performance. In this aspect, carbon materials, as build blocks, offer a great potential to play a key role in constructing advanced hybrid catalysts due to their exceptional physicochemical properties, such as high specific surface area, superior electronic conductivity, excellent stability and so on. This review summarizes the recent significant 15 progress in the design and fabrication of novel carbon-based anode catalysts via various strategies and their applications in methanol oxidation reaction. Finally, perspectives on the challenges and research trends in this emerging area are also discussed. (280 references)

1. Introduction

In the 21st century, energy crisis and environmental pollution are 20 both severe challenges faced by human society because of rapidly growing energy demand and massive combustion of fossil fuels. It is widely believed that the conventional notions of energy generation and conversion are not suitable for the world's sustainable development.[1-4] Therefore, a great deal of research 25 has been carried out to explore clean and renewable energy sources as well as their devices.[5-8] Among these different energy systems, direct methanol fuel cells (DMFCs) have been extensively studied as ideal energy converters that convert chemical energy of methanol directly to electrical energy.[9,10] 30 Moreover, as a liquid fuel at ambient conditions, methanol is low cost and is in principle renewable when sourced from biomass. Compared to pure hydrogen, methanol possesses several significant advantages: high solubility in aqueous electrolytes, high energy density and easily stored, transported, and handled 35 by the existing infrastructure.[11-13]

Nevertheless, there are two key obstacles preventing DMFCs from successful commercialization: their high manufacturing costs and sluggish kinetic rate of methanol oxidation reaction.[14] In order to address both of these challenges, an appropriate anode 40 catalyst has been regarded as the major contributor.[15,16] To date, platinum have been identified to be the efficient single-metal catalysts used for DMFCs because of their unique and excellent catalytic properties.[16,17] Unfortunately, pure Pt catalyst is readily poisoned by intermediate carbonaceous species (mainly CO) 45 during the methanol oxidation reaction, consequently leading to a sharp decrease in electrocatalytic activity.[18,19] In addition, given the fast pace of rising Pt price (*ca*. \$1600 per oz at the beginning of 2013), the dosage of Pt must be minimized in order to control the overall cost of DMFCs.

50 With respect to above concerns, to control the distribution and morphology of noble metal nanostructures on advanced supporting materials can offer effective assistance in obtaining high performance catalysts. The promising catalyst support materials should fulfill the following characteristics: (1) high 55 specific surface area and strong interaction with metal nanoparticles (NPs) to achieve high and stable dispersion; (2) excellent stability under harsh electrochemical conditions to retain the structural integrity of the composites; (3) high electrical conductivity to promote electron transfer during electrode 60 reaction process. As has been demonstrated repeatedly in experiments, the presence of supporting materials in the catalytic system can significantly enhance the electrocatalytic activity as well as reduce the noble metal consumption.[20, 21] Meanwhile, it is found that the nature of supporting materials and the distinct 65 interaction between supports and metal NPs both can affect the performance to a great extent. Therefore, choosing appropriate supporting materials and designing suitable synthetic route are essential to fuel cell technology field.

Over past decades, carbon materials have attracted immense 70 and persistent attention not only because they have extraordinary physical properties but also owing to their abundance,

processibility, environmentally friendly and relative stability in both acidic and basic media.[22,23] In nature, carbon is found free in three main allotropic forms: amorphous carbon, graphite, and diamond.[24] Depending on distinct types of crystal structures, carbon atoms can form a variety of allotropes endowed with different properties, as shown in Fig. 1. Taking 3D carbon structures as an example, the tetrahedrally arranged carbon atoms account for the hardness and transparency of diamond, while the carbon atoms in slippery and black graphite arrange in an infinite layered array. In particular, recent developments in low-dimensional carbon nanomaterials, such as 0D fullerenes, 1D carbon nanotubes (CNTs), 2D graphene etc., have further boosted the research on high-performance DMFC electrocatalyst. In comparison with traditional carbon supports, carbon nanomaterials have several unique nanometer size effects that can add attractive electrochemistry features to the resulting hybrids.[25,26]
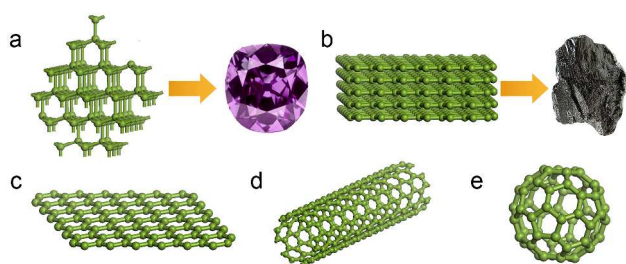
Fig. 1 Different allotropes of carbon: (a) 3D diamond, (b) 3D graphite, (c) 2D graphene, (d) 1D carbon nanotube and (e) 0D fullerene.

Actually, in such an active research field, a large number of fascinating research results related to carbon-based anode DMFC catalysts have been presented in recent years. Considering the rapidly growing attention in this intriguing area, it is of great significance to highlight the latest discoveries and achievements with a particular focus on the last three years. In this article, we review the recent advances on the design and synthesis of carbon-based electrocatalysts and their applications in anode materials for DMFCs. The remaining challenges and future prospects based on the present understandings are also discussed. It is believed that such a review article can arouse more attention towards advanced anode catalysts for DMFCs and help the readers to understand the latest advances and invigorating directions, especially for non-experts who are interested in this area.

2. Strategies for preparing carbon-based anode catalysts

So far, great efforts have been dedicated to develop new efficient synthetic methods for the preparation of electrochemical active NPs supported on carbon materials, and these efforts are not only to obtain NPs with narrow size distributions, but also to realize highly dispersed systems. Generally, these strategies can be loosely grouped into four categories: surface-functionalization methods, electrochemical deposition, electroless deposition and physical methods. Table 1 gives a summary of the average particle size of NPs in the representative carbon-based composites. These different strategies are discussed in more detail in the paragraphs below.

2.1 Surface-functionalization methods

As is well known, since the surface of intrinsic carbon materials is very inactive due to the high graphitization, it is difficult to achieve the direct deposition of highly dispersed NPs with high loading efficiency on such surface.[27,28] In order to make the inert surface active (produce more anchoring site for NPs), surface functionalization of carbon materials is usually indispensable. Generally, there are two pathways to modify the surface of carbon materials: (1) the covalent attachment of chemical groups through reactions onto the π-conjugated skeleton of carbon material and (2) noncovalent interactions or wrapping of various functional organic fragments.

2.1.1 Covalent attachments

The most commonly used covalent functionalization route is to generate binding sites, such as hydroxyl, carbonyl, and carboxyl groups on the surface of carbon materials through various oxidation treatments in acidic media.[29-32] These oxygenated functional groups can not only stabilize the dispersion of the carbon materials in polar solvents, but also provide active sites for adsorption of metal precursor. Then both the oxygen functionalities and metal precursor can be further reduced by adding some reducing agents (such as ethylene glycol, NaBH$_4$, H$_2$, formic acid etc.), leading to the formation of carbon-metal hybrids.[33-36]

A typical syn-reduction approach was reported by our group for preparing graphene-noble metal nanocomposites.[33] We first mixed graphene oxide (GO) and a metal precursor (K$_2$PtCl$_4$, K$_2$PdCl$_4$, or HAuCl$_4$·3H$_2$O) in a water-ethylene glycol system, and then the resulting suspension was put in an oil bath and heated at 100 ºC. Both GO and the metal precursor can be reduced by ethylene glycol simultaneously during the above process, forming corresponding graphene-noble metal composite. Chen and co-workers have decorated acid-treated carbon nanofiber and carbon black supports with Pt NPs of different diameters.[37] They found that an appropriate surface-oxygen group concentration was favorable to the Pt dispersion. Rojas et al. conducted a systematic study of the role of the functional groups on the CNT surface in the synthesis of PtCo/CNT composites.[38] In comparison with mild-treated CNTs, severe-treated CNTs with a larger number of oxygen-containing groups can promote the deposition of alloy particles. However, in most cases, the oxidation treatment of carbon materials would yield randomly distributed functional groups, which easily results in the agglomeration of metal NPs.[39,40] In order to overcome this barrier, carbon supports with carboxyl groups were modified with coupling molecules that can optimize the density and uniformity of metal NPs on carbon surface.[41,42] A typical example is from Wang et al.'s work, in which COOH-functionalized CNTs were reacted with imidazolium-salt-based ionic liquids (IS-ILs) in the presence of N,N'-dicyclohexylcarbodiimide (DCC), followed by the uniform loading of Pt NPs through the electrostatic interaction between the negatively charged Pt precursors and positively charged imidazolium groups (Fig. 2a).[41] It can be observed from the SEM and TEM images that high-density Pt NPs with nanoporous structures could be facilely supported on CNTs (Fig. 2b-c). In another case, Chen and co-workers synthesized Pt NPs dispersed on surface thiolation functional CNTs.[42] They demonstrated that the thiol groups directly connected to the external walls of CNTs could minimize the contact resistance as well as inhibit Pt dissolution and

coalescence.

Table 1 The average particle size of representative carbon-based anode catalysts synthesized via different methods.

Synthesis method	Precursors	Type of metal NP	Average NP size (nm)	Ref.
surface functionalization	GO, H_2PtCl_6	Pt	3–5 nm	34
surface functionalization	CNF, H_2PtCl_6	Pt	3.2 nm	36
surface functionalization	CNT, H_2PtCl_6, $CoCl_2$	PtCo alloy	2.8 ± 0.2 nm	38
surface functionalization	CNT, K_2PtCl_4, IS-ILs	Pt	3 nm	41
surface functionalization	CNT, H_2PtCl_6, NaHS	Pt	2–4 nm	42
surface functionalization	CNT, Pt^{4+}, aniline	Pt	1.9 ± 0.4	44
surface functionalization	graphite, $Pt(NO_3)_2$, NMP	Pt	2.3 nm	47
Surface functionalization	expanded graphite, $Pt(acac)_2$	Pt	3 nm	48
surface functionalization	CNT, K_2PtCl_6, [BMIM]BF_4	Pt	2.21 ± 0.21 nm	52
surface functionalization	graphite, Pt^{4+}, benzylamine	Pt	4.9 ± 2.1 nm	53
surface functionalization	expanded graphite, H_2PtCl_6, 1-Pyrenamine	Pt	3.0 nm	54
surface functionalization	CNT, H_2PtCl_6, $SnCl_4$, tetrahydrofuran	PtSn alloy	4.0 nm	55
surface functionalization	CNT, H_2PdCl_4 2-aminophenoxazin-3-one	Pd	5.8 ± 0.5 nm	56
surface functionalization	GO, K_2PtCl_4 , [BMI]	Pt	1–5 nm	58
surface functionalization	GO, H_2PtCl_6, BSA	Pt	4 nm	60
surface functionalization	CNT, H_2PtCl_6, aniline	Pt	2.0–4.0 nm	61
surface functionalization	CNT, H_2PtCl_6, aniline	Pt	3.6 nm	62
surface functionalization	GO, H_2PdCl_4 , pyrrole	Pd	6 nm	63
surface functionalization	CNT, H_2PtCl_6, dopamine hydrochloride	Pt	8 nm	66
surface functionalization	GO, H_2PtCl_6, PDDA	Pt	4.6 nm	72
surface functionalization	CNT, H_2PtCl_6, $RuCl_3$, poly(ethyleneimine)	PtRu alloy	2.5 nm	74
electrochemical deposition	expandable GO, H_2PtCl_6, H_2SO_4	Pt	15 nm	78
electrochemical deposition	GO, H_2PtCl_6, KH_2PO_4	Pt	10 nm	79
electrochemical deposition	GO, $PtCl_4$, HCl	Pt	100 nm	80
electrochemical deposition	GO, CNF, H_2PtCl_6, H_2SO_4	Pt	350–500 nm	82
electrochemical deposition	carbon paper, H_2PtCl_6, $RuCl_3$, HCl	Pt	52.9 ± 9.2 nm	81
electrochemical deposition	graphite, ZnO, K_2PtCl_6, H_2SO_4	Pt	250 nm	88
electrochemical deposition	GO, CNF, H_2PtCl_6, H_2SO_4	Pt	200–300 nm	89
electrochemical deposition	B-doped diamond, H_2PtCl_6	Pt	15 ± 5 nm	90
electrochemical deposition	Vulcan XC-72R, K_2PtCl_6, H_2SO_4	Pt	5 ± 2 nm	91
electroless deposition	graphene, copper foils, H_2PtCl_4	Pt	8–40 nm	94
electroless deposition	GO, $SnCl_2$, $PdCl_2$ and H_2PtCl_6,	Pd; Pt	5–10 nm; 2-5 nm	96
electroless deposition	CNO, H_2PtCl_6	Pt	20 nm	97
electroless deposition	CNT, $CoCl_2$, H_2PtCl_6	Pt	30–40 nm	98
physical method	GO, K_2PtCl_6	Pt	3.3-5.8 nm	103
physical method	Vulcan XC-72R, PtRu alloyed target	PtRu alloy	3.5 ± 0.5 nm	105
physical method	graphite carbon, Pt targets	Pt	4.3 nm	106
physical method	Vulcan XC-72R, Ti, Pt and Ru metal plates	PtRu alloy	2–3 nm	111
physical method	CNF, Pt target	Pt	2.6 nm	112
physical method	CNT, Pt foil, IL	Pt	2.3–3.5 nm	113
physical method	N-doped CNT, $SnCl_4$, H_2PtCl_6	Pt	1.5–4 nm	116
physical method	CNT, CeO_2 target, Pt target	Pt	2.8 ± 0.7 nm	117
physical method	CNT, Fe powder, Pt powder, H_2-Ar gas	PtFe alloy	7.1 nm	118
physical method	GO, H_2PtCl_6	Pt	2–3 nm	119
physical method	CNT, $PtCl_4$, $Co(NO_3)_2$	PtCo alloy	3.1 nm	120
physical method	nanodiamond, H_2PtCl_6, $RuCl_3$	PtRu alloy	2–4 nm	121
physical method	CNT, $PtCl_4$, $Zn(NO_3)_2$	PtZn alloy	3–5 nm	122
physical method	GO, tin porphyrin, H_2PdCl_4	Pd	10 ± 1 nm	126
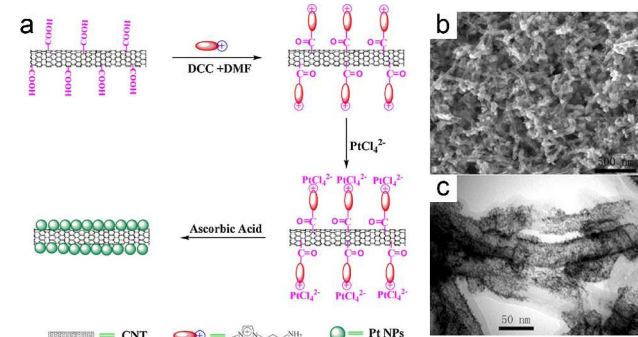
Fig. 2 (a) Illustration of the procedure for preparing CNTs/IS-ILs/Pt hybrids. DMF represents N, N-dimethylformamide. SEM (b) and TEM (c) images of CNTs/IS-ILs/Pt hybrid nanostructures. Reprinted with permission from Ref. 41, Copyright 2010, Wiley-VCH.

Nevertheless, it should be noted that such covalent functionalization would inevitably interrupt the intrinsic structure of carbon materials because of the transformation of carbon atoms from a planar sp^2-hybridized geometry to a distorted sp^3-hybridized geometry.[43,44] Although most functional groups can be eliminated by reduction, this leaves a significant amount of framework defects and small defective carbon fragments, which will continue to adversely affect the electrical, mechanical, and optical properties of the materials.[45,46] Therefore, the covalent functionalization process should be carefully designed to introduce oxygen-containing groups on the carbon materials with suitable covering density and uniform distribution. In order to efficiently avoid excessive interruption to the intrinsic structure of carbon materials, recently, a general soft-chemistry method to the synthesis of low-defect carbon materials-supported catalysts has been developed.[47] As displayed in Fig. 3a, few-layer

graphene nanoplates (GNPs) could be produced from the dispersion and exfoliation of bulk graphite in N-methyl-pyrrolidone (NMP) by a simple ultrasonic treatment, then H⁺ ions from hydrolysis of platinum nitrate in conjunction with NO_3^- were utilized to introduce an adequate amount of functional groups onto the carbon sheets. It is worth mentioning that only a very small number of structural defects in GNPs formed (Fig. 3b) because the concentration of H⁺ ions obtained from hydrolysis were much lower compared with that of traditional oxygenation processes (where strong oxidation reagents were used). In this approach, a better dispersion of Pt NPs on GNPs can be obtained compared to that of Pt NPs on reduced graphene oxide (RGO) supports (Fig. 3c-d). Most recently, Jiao et al. selected expanded graphite (EG) as a starting carbon source for making Pt/graphene hybrid.[48] Unlike GO, the graphene exfoliated from EG has fewer oxygen-containing groups, which ensures the existence of high-quality graphene with very low defects in the hybrid.

2.1.2 Noncovalent interactions

Noncovalent interactions including π-π stacking, hydrophobic forces and electrostatic attractions are also utilized to construct metal NPs-carbon hybrids.[49-51] In contrast to covalent approaches, the most advantage of noncovalent methods is that it offers the possibility of attaching electrocatalytic active NPs with minimized risk of permanently disrupting the electronic network of carbon materials.[28,49] For example, Chu et al. have stated an ionic liquids-assisted route for in situ preparation of metal NPs on purified multi-walled carbon nanotubes (MWNTs) without acid oxidation.[52] As shown in Fig. 4, the addition of a small amount of 1-butyl-3-methyl imidazolium tetrafluoroborate ([BMIM]BF₄) could result in the formation of well-crystallized and mono-dispersed metallic Pt NPs on MWNT surface. Meanwhile, the lattice of CNTs of 0.34 nm can be clearly seen from the high-resolution TEM image, implying the wall structure of MWNTs remained intact. Besides, aniline can be served as both a dispersant to debundle CNTs and a stabilizer to prepare Pt NPs.[44] Since aniline was just noncovalently absorbed on CNTs by π-π stacking, this preparation process allowed for the preservation of the intrinsic structures of CNTs. Similarly, a series of organic bifunctional molecules such as benzylamine,[53] 1-pyrenamine,[54] tetrahydrofuran,[55] 2-aminophenoxazin-3-one,[56] 1-butyl-3-methylimidazolium cholate[57,58] etc. have also been explored for fabrication of novel catalysts composing of untreated carbon materials and small metal NPs.
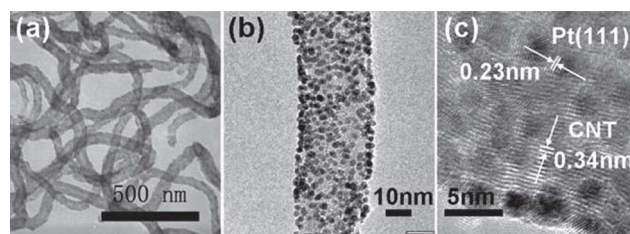
Carbon materials have been frequently wrapped by polymers with homogeneous surface functional groups to promote the deposition of metal NPs.[59-69] Guo and co-workers developed a wet-chemical procedure to synthesize 3D Pt-on-Pd bimetallic nanodendrites dispersed on poly(N-vinyl-2-pyrrolidone) (PVP)-functionalized graphene nanosheets.[59] The incorporation of PVP firstly enabled the high stability of graphene nanosheets in polar solvents, and then played an important role in the formation of Pt-on-Pd bimetallic nanodendrites. Another representative work reported by Deng's group[60] was that complex amphiphilic biopolymers such as bovine serum albumin (BSA) noncovalently bonded on GO and RGO sheets could efficiently assist in the assembly of different noble metal (Au, Pd and Pt) NPs. As depicted in Fig. 5, metal NPs were uniformly distributed on the carbon sheets, which could be explained in terms of a multiple-interaction model containing specific chemical bondings between BSA and metal NPs as well as hydrophobic and electrostatic interactions. Other interesting examples including polyaniline (PANI) as both dispersing and bonding agent for growth of Pt NPs on CNTs,[61,62] synthesis of Pd/graphene composites using polypyrrole (PPY) as a crosslinker,[63] fabrication of Pt/PPY/wetted graphene hybrids through in situ synthetic method,[64] combination of Pt/carbon black (Pt/C) and PANI nanofibers,[65] environment-friendly facile synthesis of polydopamine-modified carbon materials supported Pt NPs,[66] etc. also demonstrate the benefits from the polymer components.

As another important class of polymers, polyelectrolyte has been verified to hold great potential applications in designing metal NPs-carbon hybrids since it can substantially increase the surface charge densities of carbon materials and strengthen the electrostatic interaction with metal precursor.[70-75] Poly(diallyldimethylammonium chloride) (PDDA) has emerged as the most widely used polyelectrolyte that shows outstanding trapping capacity for the negatively charged metal precursor.[70-73] For instance, Qiu and co-workers coated GO sheets with PDDA prior to the addition of PtCl₆²⁻, thereby obtaining a Pt/graphene composite with controllable loading concentration of Pt NPs (18-78 wt%).[72] Another attractive approach was developed by Luo et al.,[71] who added NaCl to allow a random configuration of PDDA

chain during the functionalization. As a result, the high coverage of PDDA chains on graphene surface could favor electrostatic self-assembly of negatively charged $PtCl_6^{2-}$, leading to a high loading dose with enhanced dispersion uniformity of Pt NP. Except PDDA, poly(ethyleneimine) has also been employed to attach PtRu alloy NPs onto the side walls of CNTs, and the average particle size can be restricted to around 2.5 nm.[74] Furthermore, the utilization of the electrostatic attraction between two oppositely charged polyelectrolytes opens up an avenue for accessing carbon-based ultrathin multilayer films, which is known as layer-by-layer (LBL) self-assembly technique. Recently, Huang et al. constructed alternating PDDA-graphene and poly(sodium 4-styrenesulfonate) (PSS)-graphene multilayer films via a typical LBL route.[75] It was found that PDDA-graphene as the outmost layer could make $PtCl_6^{2-}$ ions easily diffuse into the film surface and result in the formation of Pt micro-nanoclusters.
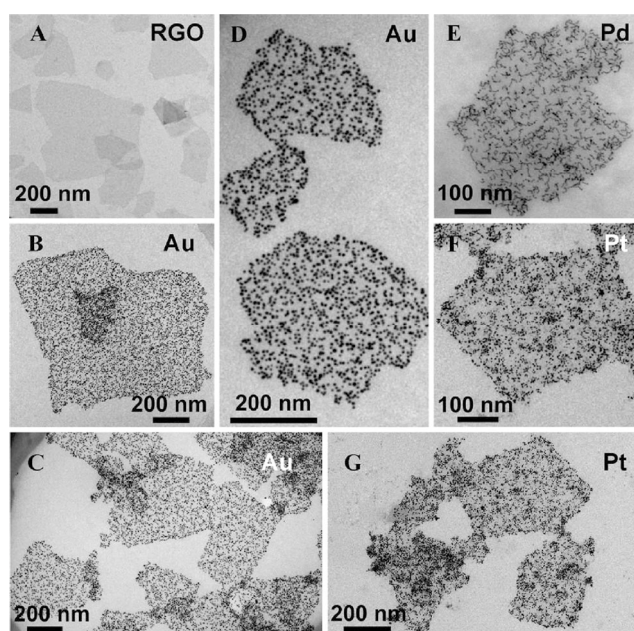
Fig. 5 TEM images of (A) BSA-RGO, (B, C, D) Au NP-BSA-RGO, (E) Pd NP-BSA-RGO, and (F, G) Pt NP-BSA-RGO. Au NPs and Pt NPs had average diameters of 6 and 4 nm, respectively. Pd NPs had a worm-like shape ~4 nm in one dimension. Reprinted with permission from Ref. 60, Copyright 2010, American Chemical Society.

Although the noncovalent routes have relatively little impact on the framework of carbon materials, one should not ignore their downsides. Because the noncovalent absorptions are inherently far weaker than covalent bonds, the metal NPs on the carbon supports are not robust and thus may easily disassemble even just by simple washing of the metal NP-carbon catalysts.[76] Moreover, an additional aftertreatment, such as reduction under high temperature with hydrogen atmosphere, is often required to obtain the final catalysts.[44,55] More importantly, most of bifunctional molecules (especially aromatic organic compounds) are highly poisonous, which should be prudently used.

2.2 Electrochemical deposition

Electrochemical deposition has been considered as a straightforward and powerful approach for loading of different metal NPs on carbon materials because there is no requirement for post-synthetic transfer of the hybrid materials.[77,78] Moreover, the nucleation and growth of metal NPs can be effectively controlled by adjusting various electrodeposition parameters, such as nucleation potential, deposition time, concentration of the metal salt, etc.[79-81] Liu and co-workers reported the synthesis of Pt/graphene nanocomposite film using a "green" synthetic route,[78] which involves three electrochemical procedures: the electrophoretic deposition of expandable graphene oxide (EGO) on indium tin oxide (ITO) surface, in situ electrochemical reduction of EGO film and electrodeposition of Pt NPs on reduced EGO film. Later, Zhou et al. proposed a one-step approach to simultaneously perform the electrochemical reduction of GO and electrodeposition of Pt NPs.[79] They demonstrated the Pt NPs prepared using the one-step method have relatively small sizes when compared with those prepared by the two-step methods.

Moreover, electrochemical deposition has also proven to be a useful technique to obtain metal NPs with a variety of shapes.[82-84] One of interesting advances is that Yao et al. designed a facile electrochemical route to prepare Pt nanoflowers modified-RGO wrapped carbon cloth (CC).[82] It can be seen from Fig. 6a-b that Pt nanoflowers deposited on RGO/CC surface appear to be well-dispersed with uniform size (350–500 nm) compared with those on bare CC substrate (200–1000 nm). Hu et al. employed this technique to synthesize a series of graphene-supported bimetallic Pt–Au nanocatalysts.[83] As shown in Fig. 6c-f, with increasing Pt/Au molar ratios, the morphology of bimetallic Pt–Au evolves from large flowerlike structures, to small flowerlike structures and finally to round particles. Alamgir's group grew monolayer-scale Pt on carbon fiber paper-supported Au nanostructures by using either potentiostatic deposition (PSD) or potential square wave deposition (PSWD).[84] For the PSD, the Au deposit took on the morphology of large urchin-like clusters with several micrometers, while for the PSWD-grown Au, there were two types of Au including urchin-like nanostructures and nanoparticles coexisting on the surface of carbon fiber paper. Other metal nanostructures such as Pt nanospikes,[85] Pt nanoparticles,[86,87] Pt nanoflowers,[80,88] Pd nanocubes,[85] PtRu nanoparticles[81,89] etc. have also been electrodeposited on different carbon materials to fabricate the corresponding composites.

The biggest weakness of electrochemical deposition method is that the deposition process usually results in large sizes and poor distribution of NPs (ranging from tens to hundreds nanometers), which are unfavorable for enhancing the utilization of active metal component. In order to overcome this problem, Ahn and co-workers controlled the particle sizes and densities of PtRu particles by altering the deposition potential, time and composition of the electrolytes.[81] It was observed that the size of PtRu particles shrunk when relatively negative potential, short deposition time and appropriate feeding ratio of Pt/Ru were applied. Yang's group combined a wet chemical synthesis route with electrochemical deposition method to produce size-controllable Pt NPs on diamond surface,[90] which is hard to be realized by direct electrodeposition. Another ingenious approach named rotating disk-slurry electrode (RoDSE) technique was developed by Santiago and co-workers.[91] By rotating a glassy carbon disk electrode in a slurry solution containing Vulcan XC-72R and K_2PtCl_6, the average particle size of Pt NPs can be

controlled to be 5 ± 2 nm. Furthermore, the combination of Pt NPs and carbon nanoonions (also known as multilayer fullerenes) was also achieved by the similar method.[92] The computational results confirmed the Pt atoms location at the surface sites of
5 carbon nanoonions.
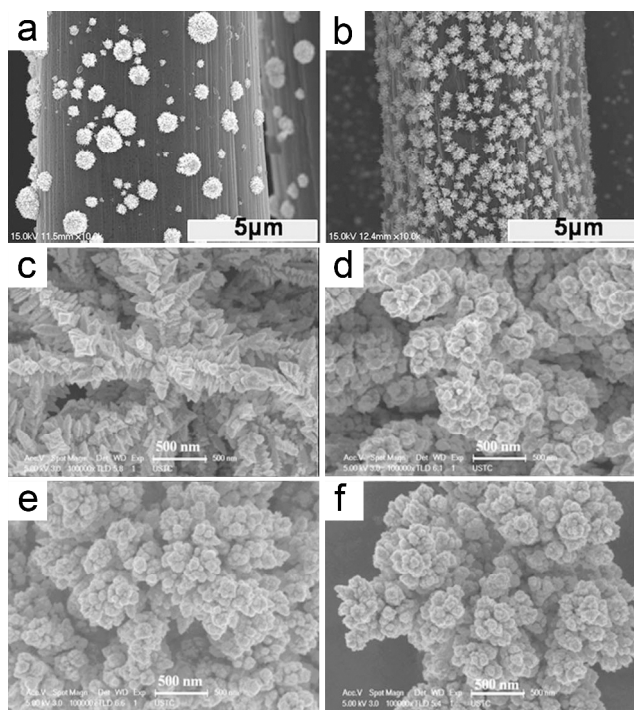
Fig. 6 SEM images of Pt nanoflowers electrodeposited on carbon cloth (a) and RGO/carbon cloth (b). Reprinted with permission from Ref. 82, Copyright 2012, Royal Society of Chemistry. Typical SEM images of the
10 Pt–Au nanostructures electrochemically deposited on the surface of the graphene/GC electrode under a constant potential of -0.4 V in 0.5 M H_2SO_4 solution containing $PtCl_6^{2-}/AuCl_4^-$ molar ratio of 0.5 : 1 (c), 1 : 1 (d), 2 : 1 (e), and 3 : 1 (f), respectively. Reprinted with permission from Ref. 83, Copyright 2011, Royal Society of Chemistry.

15 **2.3 Electroless deposition**

Metal nanocrystals with higher reduction potential (such as Pt and Au) can form spontaneously on carbon materials by electroless deposition, and this phenomenon happens due to the direct redox reaction via electron transfer between the metal ions
20 and the carbon supports.[93] Since such a process does not require any external reducing agents, electroless deposition has been recognized as a green strategy to produce metal NPs with clean surface and large facial areas.[94] However, this method is feasible only when the redox potential of carbon supports is lower than
25 that of metal ions. Therefore, the majority of metal cations including Ag^+, Ni^{2+}, Cu^{2+} etc. could not be reduced to metal by this way because of their lower redox potentials, which restricts the application of electroless deposition to a large extent.[27,50]

To conquer this challenge, Dai's group proposed an innovative
30 substrate-enhanced electroless deposition (SEED) method for functionalization of CNTs with almost all of metal NPs,[95] where the metal substrate whose redox potential is lower than that of the metal ion is able to act as an anode, while the CNTs only serve as cathodes and templates for metal deposition. This SEED method
35 can also be extended to fabricate other metal/carbon hybrids. For instance, Liu et al. have synthesized a number of metal (M)-

graphene nanocomposites (M= Pt, Ag, Pd, Au etc.) based on the similar principle.[94] As shown in Fig. 7a-c, the external surface of metal (Cu or Zn) foils were coated with graphene sheets, and
40 subsequently, the modified foils were immersed into solutions containing different metal precursors, forming the corresponding metal/graphene hybrid materials. In another example, the oxygen-containing functional groups of GO can also be sensitized directly by Sn^{2+} ions,[96] which are efficient to reduce Pt^{2+} or Pd^{2+}
45 ions and thus make it possible to form well-dispersed Pt or Pd NPs on graphene sheets (Fig. 7d-e).
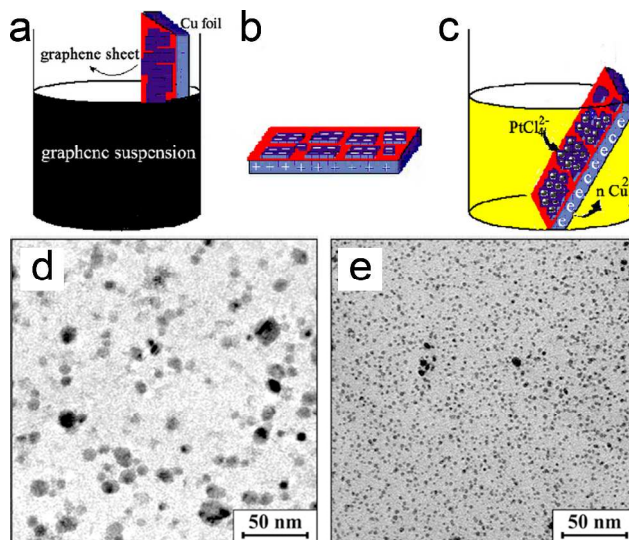
Fig. 7 Schematic illustration for (a) preparing Cu foil-supported GS substrate, (b) charge redistribution on Cu foil-supported GS substrate, and
50 (c) Pt nanoparticle deposition process. Reprinted with permission from Ref. 94, Copyright 2011, Elsevier B.V. TEM images of G-Pd (d) and G-Pt (e), respectively. Reprinted with permission from Ref. 96, Copyright 2013, American Chemical Society.

On the other hand, recent studies indicated that the
55 pretreatment of carbon materials prior to electroless deposition has a great effect on the sizes and shapes of metal NPs.[97,98] Raston's group reported the use of plasma-treated carbon nanoonions as the starting materials for anchoring Pt NPs with the assistance of shear flow.[97] TEM observations revealed that
60 there was an improvement in the homogeneity of Pt NPs decorated on the plasma-treated carbon nanoonions relative to those on the pristine materials. Another interesting modification is that Geng et al. utilized polymer-wrapped CNTs together with $CoCl_2$ to prepare single-crystal platinum nanocubes/CNTs
65 heterostructures via electroless deposition processes.[98] They also demonstrated that this method could be employed to prepare other noble metal nanocubes dispersed on CNTs.

2.4 Physical methods

An alternative way to prepare DMFC anode catalysts is to load
70 electrocatalytic active NPs on carbon supports through the use of physical methods, which can be divided into two major classes: (1) gas-phase deposition and (2) irradiation-assisted technique. For the former, gas-phase deposition allows the modification of substrates with a great variety of metal NPs and provides high-
75 degree control over their microstuructures.[99-101] Meanwhile, the catalyst deposit is localized directly at the membrane/electrode

interface, which is beneficial to increase the catalyst utilization.[102] As to the latter, the essential feature of irradiation-assisted technique is that it serves to remarkably accelerate the synthetic processes and enables the reduction of most metal ions to zero
5 valent state.[103,104]

2.4.1 Gas-phase deposition

For the past few years, magnetron sputtering has emerged as the most common gas-phase technique to prepare metal/carbon hybrids.[99,105] Fig. 8a is an illustration of the basic components of
10 a sputter chamber,[105] which consists of a turbo molecular pump, a powder sample holder ("wheel") and an orthogonally oriented sputter gun. By using this instrument, Dameron et al. succeeded in sputtering PtRu NPs to the surface of a carbon matrix support (Fig. 8b-c). This "dry" processing technique is able to eliminate
15 the need for drying and purification steps and also avoids the use of toxic or flammable materials. In addition, one can accurately tune the structures and composition of the products by changing any one of sputtering parameters, such as the output power, sputtering time, gas pressure, etc. A representative example is
20 described by Shang and co-workers.[99] By selecting different sputtering time, porous graphene nanoflake films could be covered with Pt nanoclusters of varying thickness ranging from 2.1 to 85.0 nm. In this context, a great number of metal nanostructures have been composited with carbon materials and
25 their derivatives via magnetron sputtering, which include Pt/C,[106] Pt-based alloy/C,[107-109] PtRu/N-doped C,[110] PtRu/TiO$_2$/C,[111] Pt/CNFs,[112] Pt/ionic liquids/CNTs,[113] Pt/CeO$_2$/CNTs,[114] etc.
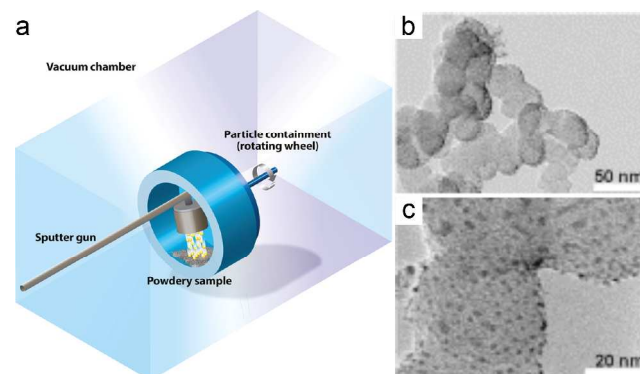
Fig. 8 (a) Illustration of custom vacuum instrumentation used to fabricate
30 powder catalysts. (b,c) TEM images of typical sputtered catalyst materials. Reprinted with permission from Ref. 105, Copyright 2011, American Chemical Society.

Atomic layer deposition (ALD) is another effective method for the coating of nanostructured metal catalysts on complex
35 supports.[100,101,115,116] A very interesting finding was reported by Bent's group,[101] who showed that ALD could deposit Pt nanowires of controllable diameter on highly ordered pyrolytic graphite (HOPG). It is clearly seen from Fig. 9 that the growth of Pt took place only on the step edges of HOPG and the height and
40 width of Pt nanowires could be adjusted simultaneously by adjusting the number of ALD cycles. Most recently, Perng et al. have demonstrated that the formation of Pt/ZnO catalysts on carbon cloth can be achieved by a combination of hydrothermal and ALD methods.[115] They found that the ZnO seed layer coated
45 by ALD facilitated the adhesion of hydrothermally grown ZnO nanorobs on carbon cloth, and then the photoinduced hydrophilicity of the ZnO surface could further assist the

deposition of well-dispersed Pt NPs. Besides, other gas-phase deposition methods, such as pulsed laser deposition,[117] arc
50 discharge evaporation,[118] etc. have also been introduced to prepare carbon-based catalysts.
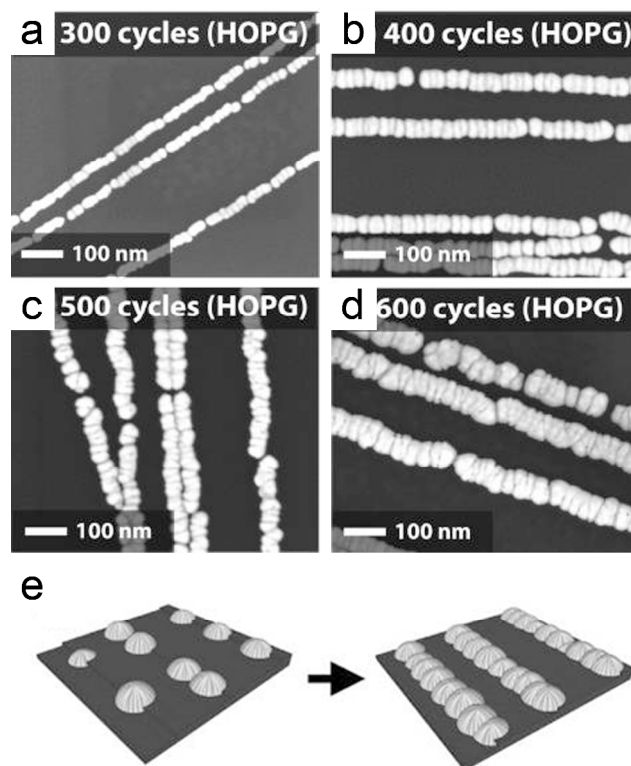
Fig. 9 (a-d) Plan-view SEM images of ALD Pt on HOPG. (e) A visualization of the nucleation and formation mechanism of Pt nanowires.
55 Reprinted with permission from Ref. 101, Copyright 2013, American Chemical Society.

2.4.2 Irradiation-assisted methods

Among different irradiation-assisted methods for synthesizing metal NPs/carbon hybrids, the microwave-assisted polyol method
60 is of particular interest due to its merits of safe, speed, energy efficiency, and implementation simplicity.[103,119-124] One typical case is that Papakonstantinou's group reported the fabrication of Pt/RGO electrocatalysts by a one-pot co-reduction microwave-assisted approach.[103] After an ultrafast microwave irradiation (50-
65 100 s), the Pt nanocrystals could be distributed quite uniformly on the surface of the reduced carbon sheets (Fig. 10a-c). In order to better understand the microwave process, Ravishankar et al. conducted a detailed investigation of the mechanism of the formation of the Pt/RGO hybrids.[119] As illustrated in Fig. 10d,
70 microwave irradiation polarizes the electron cloud and agitates the dipoles related to oxygen-containing groups, thus creating active hot spots on the GO sheets, which can reduce the precursor Pt^{4+} to Pt^{2+} in the presence of ethylene glycol. These nucleated Pt^{2+} ions may reduce GO, thereby getting oxidized back to Pt^{4+}
75 and meanwhile resulting in the generation of defect sites on the graphene basal plane, which can act as nucleation centers for the subsequent formation of Pt NPs by EG reduction.
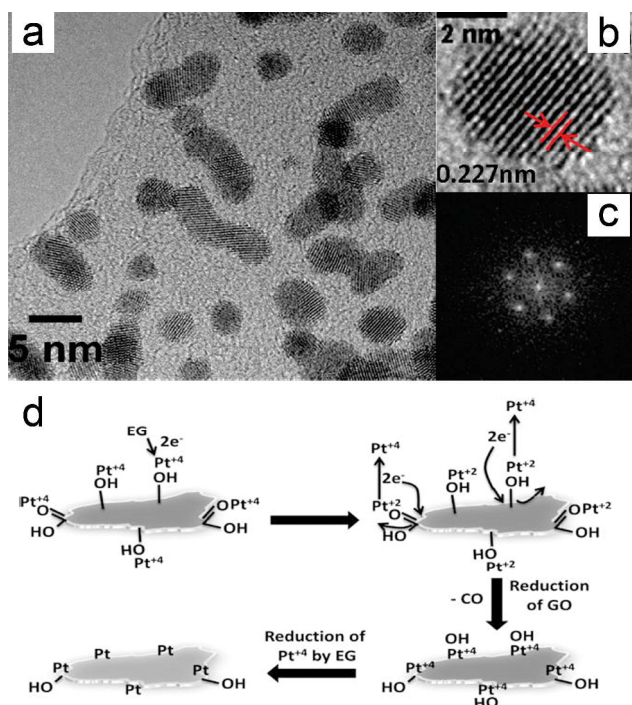
Fig. 10 (a) TEM image of Pt/RGO synthesized by employing a one-pot microwave-assisted approach. (c) HRTEM image and fast fourier transforms (FFTs) of a single Pt NP. Reprinted with permission from Ref. 103, Copyright 2010, American Chemical Society. (d) Schematic representation of synergistic co-reduction of GO and Pt-salt under microwave radiation. Reprinted with permission from Ref. 119, Copyright 2011, American Chemical Society.

Beyond microwave, other radioactive sources were also used to promote the deposition of metal NPs on carbon materials.[125,126] As an example, Haram et al. presented γ-radiolysis-assisted preparation of a composite composed of CNTs and Pt NPs.[125] The main advantage of this route is that it does not need any reducing agents because the γ-radiolysis of water produces hydrated electrons, which can efficiently reduce Pt^{4+} ion. A much greener photocatalytic method for the synthesis of highly dispersed Pd NPs on RGO surface was reported by Sun et al.[126] They found that both GO and Pd^{2+} could be successfully reduced by using tin (IV) porphyrin as a photocatalyst under visible light irradiation (λ > 400 nm).

3. Applications of carbon-based catalysts in methanol oxidation reactions

The high-efficiency methanol oxidation reaction depends largely on the performance of anode catalysts in terms of high electrocatalytic activity, good poison tolerance and reliable stability.[17,127] There is no doubt that the use of carbon-based catalysts is the mainstream in this area. On the basis of different compositions, the recently developed carbon-based anode catalysts can be divided into five classes: single-carbon, multiple-carbon, heteroatom-doped carbon, metal oxide-modified carbon and polymer-modified carbon supported catalysts. These carbon-based composite catalysts and their electrochemical

properties toward methanol oxidation are listed in Table 2 and will be systematically discussed in the following sections.

3.1 Single-carbon supported catalysts

3.1.1 Carbon black

As one of the products manufactured by pyrolyzing petroleum hydrocarbon, carbon black is a widely used material for electrocatalytic-related applications owning to its high availability and low cost.[23] Common carbon blacks include acetylene black, Vulcan XC-72, Ketjen Black, etc., which possess different physicochemical characteristics, such as specific surface area, electronic conductivity, surface to volume ratio, stability and surface functionality.[128,129] In this aspect, Vulcan XC-72 has been proven to be a superior support since it has a relatively high specific surface area and passable electronic conductivity.[130,131] On the contrary, the low surface area of acetylene black and the high surface resistance of Ketjen Black make them difficult to serve as supporting materials.[132]

Salgado et al. investigated the performance of PtRu electrocatalysts supported by different carbon materials containing Vulcan XC-72 and HNO_3-functionalized Vulcan XC-72.[133] They found that the highest power density attained with HNO_3-treated Vulcan XC-72-based electrode, revealing that the presence of oxygenated groups on Vulcan XC-72 had obvious effects on the methanol oxidation reaction. Carbon black can also act as a universal platform for loading active metal NPs with controllable compositions and shapes.[134-137] For instance, the fabrication of bimetallic PtNi electrocatalysts with different Pt/Ni atomic ratios supported on Vulcan XC-72 was reported by Sun and co-workers.[134] The electrochemical measurements showed that the corresponding hybrid with Pt/Ni ratio of 3:1 possessed markedly enhanced specific activities and decreased CO adsorption relative to Pt/Vulcan XC-72 catalyst. Wu's group deposited Pt atoms on commercially available PtRu/carbon black (PtRu/C) by a displacement reaction route.[135] The electrocatalytic abilities of the as-obtained sub-monolayered and monolayered Pt-modified PtRu/C have been remarkably improved, mainly due to the increased Pt content on the catalyst surface. Zeng prepared polyhedra Pt NPs decorated Vulcan XC-72 composite and tested its catalytic performance.[136] Besides the improved CO tolerance, the mass activity (575 mA mg^{-1}) of the resulting catalyst increased 55% compared to Pt/C from E-TEK (370 mA mg^{-1}).

3.1.2 Mesoporous carbon (MC)

Although Vulcan XC-72 supported catalysts usually exhibit improved electrocatalytic properties, the large amount of microporosity (pore sizes < 2 nm) in Vulcan XC-72 inevitably decreases the efficiency of catalysts due to the difficulty in reactant accessibility.[132,138] On the other hand, macroporous carbon materials (pore sizes > 50 nm) possess good mass transport characteristics but small surface areas and low electrical conductivity.[130] In order to balance these desirable features, MCs (2 nm < pore sizes < 50 nm) have incurred intense interest in fuel cell applications since they can facilitate the transport of reactants to the electrocatalysts and simultaneously exhibit large surface areas and low charge-transfer resistance.[138-143]

Table 2 The electrocatalytic properties of representative carbon-based anode catalysts with different compositions toward methanol oxidation reactions.

Catalyst composition	Testing conditions	ECSA	Specific/Mass activity	I_F/I_R	Ref.
PtNi/C	1 M NaOH and 1 M CH$_3$OH, 50 mV s^{-1}	33.6 m^2 g^{-1}	48.5 mA cm^{-2}	-	134
Pt/C	0.5 M H$_2$SO$_4$ and 1 M CH$_3$OH, 20 mV s^{-1}	-	575 mA mg^{-1}	-	136
Pt/MC	0.5 M H$_2$SO$_4$ and 0.5 M CH$_3$OH, 50 mV s^{-1}	27.0 m^2 g^{-1}	250 mA mg^{-1}	-	139
PtRu/MC	0.5 M H$_2$SO$_4$ and 1 M CH$_3$OH, 50 mV s^{-1}	-	487.9 mA mg^{-1}	3.3	140
PtRu/MC	0.5 M H$_2$SO$_4$ and 1 M CH$_3$OH, 10 mV s^{-1}	64.1 m^2 g^{-1}	19.8 mA mg^{-1}	-	138
Pt/CNF	0.5 M H$_2$SO$_4$ and 0.5 M CH$_3$OH, 50 mV s^{-1}	42.1 m^2 g^{-1}	410 mA mg^{-1}	-	36
Pt/CNF	0.5 M H$_2$SO$_4$ and 1 M CH$_3$OH, 10 mV s^{-1}	-	276 mA mg^{-1}	6.99	150
Pt/CNT	1 M H$_2$SO$_4$ and 2 M CH$_3$OH, 20 mV s^{-1}	116.1 m^2 g^{-1}	47.4 mA cm^{-2}	2.94	159
PtRu/CNT	0.5 M H$_2$SO$_4$ and 0.5 M CH$_3$OH, 50 mV s^{-1}	215 m^2 g^{-1}	205 mA cm^{-2}	1.39	160
PdMo/CNT	1 M KOH and 1 M CH$_3$OH, 50 mV s^{-1}	38.4 m^2 g^{-1}	395.6 mA mg^{-1}	-	161
PtCo/CNT	1 M H$_2$SO$_4$ and 2 M CH$_3$OH, 20 mV s^{-1}	106.0 m^2 g^{-1}	428.0 mA mg^{-1}	1.29	162
PdPtCu/CNT	0.5 M H$_2$SO$_4$ and 1 M CH$_3$OH, 50 mV s^{-1}	-	94.4 mA cm^{-2}	2.41	163
PtZn/CNT	0.5 M H$_2$SO$_4$ and 1 M CH$_3$OH, 50 mV s^{-1}	12.0 m^2 g^{-1}	-	1.51	122
PtIr/CNT	0.5 M H$_2$SO$_4$ and 0.5 M CH$_3$OH, 50 mV s^{-1}	97.8 m^2 g^{-1}	311 mA mg^{-1}	1.08	164
Pt/graphene	0.5 M H$_2$SO$_4$ and 1 M CH$_3$OH, 50 mV s^{-1}	36.3 m^2 g^{-1}	-	0.83	174
PtRu/graphene	0.5 M H$_2$SO$_4$ and 1 M CH$_3$OH, 50 mV s^{-1}	-	205.7 mA mg^{-1}	4.70	181
PtPd/graphene	0.1 M HClO$_4$ and 1.0 M CH$_3$OH, 50 mV s^{-1}	19.7 m^2 g^{-1}	198 mA mg^{-1}	1.61	183
PtAu/graphene	0.5 M H$_2$SO$_4$ and 0.5 M CH$_3$OH, 50 mV s^{-1}	82.2 m^2 g^{-1}	394 mA mg^{-1}	1.25	83
PtCo/graphene	1 M H$_2$SO$_4$ and 2 M CH$_3$OH, 20 mV s^{-1}	75.8 m^2 g^{-1}	35.8 mA cm^{-2}	1.28	184
PtFe/graphene	0.5 M H$_2$SO$_4$ and 1 M CH$_3$OH, 50 mV s^{-1}	16.5 m^2 g^{-1}	3.55 mA cm^{-2}	-	186
PtSn/graphene	0.5 M H$_2$SO$_4$ and 0.5 M CH$_3$OH, 50 mV s^{-1}	-	16.21 mA cm^{-2}	2.18	189
PtCu/graphene	0.1 M H$_2$SO$_4$ and 2 M CH$_3$OH, 50 mV s^{-1}	75.6 m^2 g^{-1}	780 mA mg^{-1}	1.75	194
PtRu/graphene	1 M H$_2$SO$_4$ and 2 M CH$_3$OH, 40 mV s^{-1}	158 m^2 g^{-1}	33.5 mA mg^{-1}	4.7	195
Pd/graphene	0.5 M NaOH and 1 M CH$_3$OH, 50 mV s^{-1}	83.0 m^2 g^{-1}	61.6 mA cm^{-2}	-	196
Pt/3D graphene	0.5 M H$_2$SO$_4$ and 1 M CH$_3$OH, 50 mV s^{-1}	-	1.6 mA cm^{-2}	2.25	197
Pt/3D graphene	0.5 M H$_2$SO$_4$ and 1 M CH$_3$OH, 50 mV s^{-1}	16.8 m^2 g^{-1}	2.5 mA cm^{-2}	1.13	198
Pt/aerogel	0.5 M H$_2$SO$_4$ and 2 M CH$_3$OH, 50 mV s^{-1}	87.4 m^2 g^{-1}	395.3 mA mg^{-1}	-	199
PtAu/CP	0.5 M H$_2$SO$_4$ and 1 M CH$_3$OH, 50 mV s^{-1}	215 m^2 g^{-1}	1340 mA mg^{-1}	-	200
Pt/CNT/C	0.5 M H$_2$SO$_4$ and 1 M CH$_3$OH, 20 mV s^{-1}	102.5 m^2 g^{-1}	9.6 mA cm^{-2}	-	205
Pt/CNF/graphene	0.5 M H$_2$SO$_4$ and 1 M CH$_3$OH, 50 mV s^{-1}	34.8 m^2 g^{-1}	468 mA mg^{-1}	1.09	208
Pt/MC/graphene	0.5 M H$_2$SO$_4$ and 0.5 M CH$_3$OH, 50 mV s^{-1}	-	81.6 mA mg^{-1}	1.33	209
PtRu/CNT/graphene	0.5 M H$_2$SO$_4$ and 1 M CH$_3$OH, 20 mV s^{-1}	118.69 m^2 g^{-1}	136.7 mA mg^{-1}	6.33	211
Pt/CNT/graphene	0.5 M H$_2$SO$_4$ and 1 M CH$_3$OH, 20 mV s^{-1}	77.39 m^2 g^{-1}	11.1 mA cm^{-2}	-	214
Pt/N-doped PCN	0.5 M H$_2$SO$_4$ and 1 M CH$_3$OH, 50 mV s^{-1}	24.6 m^2 g^{-1}	343 mA mg^{-1}	-	224
Pt/N-doped C	0.5 M H$_2$SO$_4$ and 1 M CH$_3$OH, 50 mV s^{-1}	33.14 m^2 g^{-1}	103 mA mg^{-1}	1.86	225
Pt/N-doped CNT	0.5 M H$_2$SO$_4$ and 1 M CH$_3$OH, 20 mV s^{-1}	64.3 m^2 g^{-1}	13.2 mA cm^{-2}	-	226
PtAu/N-doped graphene	0.5 M H$_2$SO$_4$ and 0.5 M CH$_3$OH, 50 mV s^{-1}	60.9 m^2 g^{-1}	417 mA mg^{-1}	1.21	220
Pt/N-doped graphene	0.5 M H$_2$SO$_4$ and 0.5 M CH$_3$OH, 20 mV s^{-1}	80.45 m^2 g^{-1}	24.94 mA cm^{-2}	-	232
Pt/B-doped CNT	0.5 M H$_2$SO$_4$ and 0.5 M CH$_3$OH, 10 mV s^{-1}	55.7 m^2 g^{-1}	13.6 mA cm^{-2}	-	234
Pt/S-doped CNT	0.5 M H$_2$SO$_4$ and 1 M CH$_3$OH, 20 mV s^{-1}	88.4 m^2 g^{-1}	862.8 mA mg^{-1}	-	236
PtCo/S-doped CNT	0.5 M H$_2$SO$_4$ and 1 M CH$_3$OH, 20 mV s^{-1}	129.5 m^2 g^{-1}	1302.1 mA mg^{-1}	0.83	237
Pt/Sn-modified CNT	0.5 M H$_2$SO$_4$ and 1 M CH$_3$OH, 50 mV s^{-1}	17.2 m^2 g^{-1}	91.0 mA mg^{-1}	2.2	238
Pt/CeO$_2$/graphene	0.5 M H$_2$SO$_4$ and 1 M CH$_3$OH, 50 mV s^{-1}	66.4 m^2 g^{-1}	440.1 mA mg^{-1}	1.48	243
Pt/CeO$_2$/graphene	0.5 M H$_2$SO$_4$ and 1 M CH$_3$OH, 100 mV s^{-1}	75.6 m^2 g^{-1}	366 mA mg^{-1}	1.59	245
Pt/CeO$_2$/C	0.5 M H$_2$SO$_4$ and 1 M CH$_3$OH, 20 mV s^{-1}	51 m^2 g^{-1}	14.6 mA cm^{-2}	-	246
PtRu/MnO$_2$/CNT	1 M HClO$_4$ and 1 M CH$_3$OH, 100 mV s^{-1}	112 m^2 g^{-1}	906 mA mg^{-1}	-	251
Pt/MnO$_2$/graphene	1 M H$_2$SO$_4$ and 2 M CH$_3$OH, 20 mV s^{-1}	103.2 m^2 g^{-1}	1224 mA mg^{-1}	1.23	255
Pd/MnO$_2$/CNT	0.5 M NaOH and 1 M CH$_3$OH, 50 mV s^{-1}	35.57 m^2 g^{-1}	432.02 mA mg^{-1}	18.3	253
Pd/MnO$_2$/graphene	0.5 M KOH and 1 M CH$_3$OH, 50 mV s^{-1}	-	20.4 mA cm^{-2}	4.3	254
Pd/MnO$_2$/graphene	0.5 M NaOH and 1 M CH$_3$OH, 50 mV s^{-1}	82.6 m^2 g^{-1}	838 mA mg^{-1}	-	256
Pt/TiO$_2$/graphene	0.5 M H$_2$SO$_4$ and 1 M CH$_3$OH, 20 mV s^{-1}	79.1 m^2 g^{-1}	83.1 mA cm^{-2}	-	261
Pt/TiO$_2$/graphene	0.5 M H$_2$SO$_4$ and 1 M CH$_3$OH, 5 mV s^{-1}	62.8 m^2 g^{-1}	42.3 mA cm^{-2}	1.24	265
Pt/TiO$_2$/C	0.5 M H$_2$SO$_4$ and 0.5 M CH$_3$OH, 50 mV s^{-1}	65.3 m^2 g^{-1}	102.8 mA mg^{-1}	-	266
PtRu/TiO$_2$/CNF	0.5 M H$_2$SO$_4$ and 2 M CH$_3$OH, 20 mV s^{-1}	427 m^2 g^{-1}	516 mA mg^{-1}	-	264
Pt/CuO/C	0.5 M H$_2$SO$_4$ and 0.3 M CH$_3$OH, 10 mV s^{-1}	87.1 m^2 g^{-1}	85.48 mA cm^{-2}	3.2	269
Pt/Mn$_3$O$_4$/CNT	0.5 M NaOH and 1 M CH$_3$OH, 50 mV s^{-1}	64.8 m^2 g^{-1}	970.2 mA mg^{-1}	1.02	270
Pt/WO$_3$/MC	0.5 M NaOH and 1 M CH$_3$OH, 25 mV s^{-1}	80.6 m^2 g^{-1}	410 mA mg^{-1}	-	272
Pt/PANI/CNT	0.5 M H$_2$SO$_4$ and 1 M CH$_3$OH, 10 mV s^{-1}	110.2 m^2 g^{-1}	-	1.62	62
PtRu/PANI/CNT	0.1 M H$_2$SO$_4$ and 1 M CH$_3$OH, 50 mV s^{-1}	147.55 m^2 g^{-1}	622.69 mA mg^{-1}	7.55	68
Pd/PPY/graphene	0.5 M NaOH and 1 M CH$_3$OH, 50 mV s^{-1}	41.8 m^2 g^{-1}	359.8 mA mg^{-1}	7.3	63
Pt/PDDA/graphene	1 M H$_2$SO$_4$ and 2 M CH$_3$OH, 50 mV s^{-1}	141.6 m^2 g^{-1}	2.53 mA cm^{-2}	1.92	72
Pt/PDDA/GO	1 M H$_2$SO$_4$ and 2 M CH$_3$OH, 50 mV s^{-1}	66 m^2 g^{-1}	3.82 mA cm^{-2}	3.32	73
PtRu/PEI/CNT	0.5 M H$_2$SO$_4$ and 1 M CH$_3$OH, 50 mV s^{-1}	91.4 m^2 g^{-1}	636 mA mg^{-1}	-	74
PtRu/HPAs-CS/ graphene	0.5 M H$_2$SO$_4$ and 1 M CH$_3$OH, 20 mV s^{-1}	73.4 m^2 g^{-1}	232 mA mg^{-1}	-	279

Su et al. demonstrated that the utilization of Pt/ordered MC (Pt/OMC) catalyst showed a significantly higher electrochemically active surface area (ECSA) (27.0 m g^{-1}) in methanol electrooxidation than that of Pt/microporous carbon black BP2000 (24.4 m g^{-1}) and commercial E-TEK catalysts (19.1 m g^{-1}),[139] suggesting the abundant mesoporous structures in carbon support played an important role in the liquid-phase

electrochemical reaction. Moreover, the influence of pore size of MC on the electrochemical performance of the anode has been studied by Maiyalagan and co-workers.[140] They found that the PtRu NPs dispersed on highly ordered MC (HOMC) with relatively larger mesopores had advantages in electrochemical activity, poison tolerance and stability. Similarly, Sun et al. synthesized two kinds of graphitic MCs (GMC-1 and GMC-2) with different pore sizes by adjusting the amount of the graphitization catalyst.[138] They showed that the maximum power density (210 mW cm^{-2}) of the DMFC with PtRu/GMC-2 as the anode was 62% and 24% higher than those with PtRu/GMC-1 (130 mW cm^{-2}) and the commercial PtRu/Vulcan XC-72 (170 mW cm^{-2}), respectively, which was attributed to the faster mass transfer in anode catalyst layers benefiting from the GMC-2 support with higher percentage of pores above 20 nm.

In order to further optimize the catalytic performance of MC-based composites, it is necessary to regulate the surface characteristics of the MC through different surface modification methods prior to the deposition of metal NPs.[132,144] Park et al. performed the chemical modifications of MC at different pH to examine their influence on electrochemical performance for DMFCs.[144] With increasing the pH value, the electrocatalytic activity of MC-supported PtRu catalysts was enhanced, resulting from higher loading and dispersion as well as smaller size of PtRu NPs. In another study, MC xerogels were submitted to different oxygen functionalization treatments including diluted and concentrated nitric acid as well as gas-phase 5% O$_2$-N$_2$ oxidation.[132] The results indicated that gas-phase functionalization could introduce more basic functionalities on the carbon surface which enhanced PtRu active-phase dispersion and its alloying degree, thus achieving an enhanced mass activity of 683 mA mg^{-1}.

3.1.3 Carbon nanofibers (CNFs)

As a kind of 1D carbon materials, CNFs have also been used as the supports for metal NPs.[39,145,146] There are three types of CNFs which differ for the disposition of the graphene layers: platelet, ribbon, and herring-bone.[147,148] Generally, most CNFs present specific surface area from 10 m^2 g^{-1} to 200 m^2 g^{-1}, showing no superiority over traditional carbon supports such as Vulcan XC-72 (~250 m^2 g^{-1}).[149] In fact, the main advantage of CNFs is their negligible micropore content, which can host more accessible active sites during the catalytic reactions.[31]

Lim and co-workers fabricated the CNF-supported PtRu catalysts and examined their chemical stability and durability for methanol oxidation reaction.[145] In comparison to a commercial Pt/C catalyst, the PtRu/CNF hybrids measured lower in terms of the decay rate of the cell voltage and the difference of the anode potential after long-term durability testing, which were probably linked to the strong interaction between the surface of the CNF and the PtRu alloy NPs. Another study from Kallio et al.'s work also demonstrated the stable nature of the anode layer structure of CNF-supported catalysts.[146] During the 6-day-long fuel cell stability tests, the current density change of CNF-based electrode was almost negligible, which was clearly better than those of Vulcan XC-72 and few-walled CNT-based electrodes.

Additionally, the reasonable control of the loading mass and distribution of metal NPs on CNF surface could further enhance the electrocatalytic activity.[36,150] Huang et al. used inexpensive electrospun CNFs as starting materials to synthesize Pt/CNF

nanocomposites with different morphologies and Pt loading amounts.[36] In particular, the Pt/CNF electrocatalyst with 49 wt% Pt loadings exhibited better electrocatalytic properties (410 mA mg^{-1}) than other Pt/CNF composites and E-TEK Pt/C catalyst. Dempsey et al. reported that the effective utilization of both outer and inner sides of CNFs could enable good dispersion and efficient impregnation of Pt NPs all along the nanofibers.[150] This unique structure could provide stability against poisoning species and result in excellent response towards methanol oxidation reaction.

3.1.4 Carbon nanotubes (CNTs)

CNTs have been undoubtedly an important member in the family of nanostructured carbons, which can be considered as a seamless cylinder formed by rolling one or more layers of graphene (denoted as SWNT or MWNT, respectively) with open or closed ends.[151,152] Owing to their incredible electrical and structural characteristics, such as high external surface, good electronic conductivity, large surface to volume ratio, and high chemical stability, CNTs have shown very exciting results in catalyst support for fuel cell applications in the last decade.[153-155]

Gattia and co-workers loaded Pt clusters by an impregnation process on three carbon supports containing MWNTs, single-wall carbon nanohorns (SWNH), and Vulcan XC-72, respectively.[156] Electrochemical characterization reflected that Pt particles deposited on MWNTs were much efficient than those on other carbon supports in the methanol oxidation reaction, implying MWNT is a promising candidate material for DMFCs. Similar to the cases of other carbon-metal NPs systems, CNTs subjected to different pretreatment methods have a marked influence on catalytic activity of matal NPs.[52,157] In this aspect, Piela et al. pretreated the MWNTs by either high-temperature KOH etching or annealing (graphitization) and investigated their properties as the conductive supports for catalytic metal NPs in DMFCs.[157] Among the different MWNT supports, the graphitized, entangled MWNTs offered the best performance comparable to the commercial E-TEK catalyst, which was resulted from the optimum combination of metal utilization and transport properties as well as the improved conductivity. Jiang and co-workers successfully synthesized functional mesoporous carbon nanotubes (MCNTs) and developed their integration with Pt nanocrystals (Pt/MCNTs), as can be seen from Fig. 11a.[158] Whether for the forward anodic peak current density (I$_F$) or the ratio of the forward anodic peak current to the reverse anodic peak current (I$_F$/I$_R$), Pt/MCNTs had strong advantages over the Pt/closed CNTs (Pt/CCNTs) and E-TEK catalysts (Fig. 11b). Another interesting example is that our group reported the synthesis of Pt/MWNT nanocomposites by a straightforward soft chemical route, which can avoid cumbersome acid treatment and introduce only a very small amount of defects to the external walls of the MWNTs.[159] As shown in Fig. 11c-d, the as-derived small Pt NPs on low-defect MWNTs (PtLM) exhibited high electrocatalytic activity (47.4 mA cm^{-2}) and excellent CO-poisoning tolerance (I$_F$/I$_R$ value of as high as 2.94) for methanol oxidation, far outperforming the Pt-acid treated MWNT (PtAM) electrocatalysts.
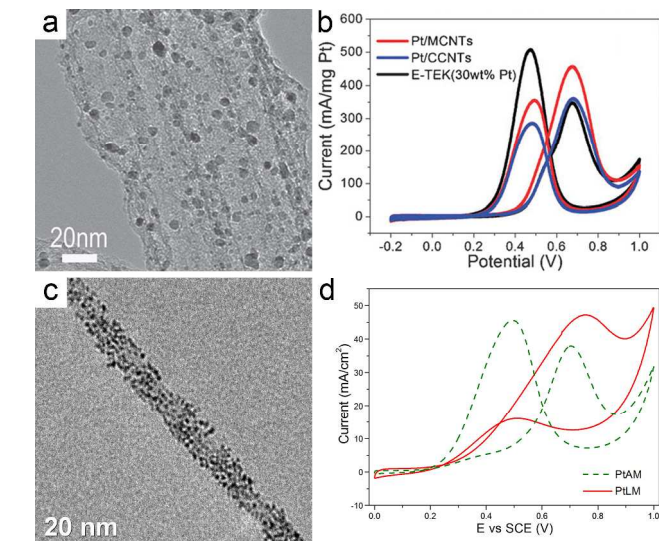
Fig. 11 (a) High-magnification TEM images of Pt NPs supported on MCNTs. (b) CV curves recorded at 20 mV s^{-1} of methanol electrooxidation on the Pt/MCNTs, Pt/CCNTs and commercial E-TEK (30 wt% Pt) catalysts at room temperature, respectively. Reprinted with permission from Ref. 158, Copyright 2011, Royal Society of Chemistry. (c) TEM image of PtLM hybrid with when the feeding ratio of Pt/MWNTs is 6:1. (d) CVs of PtAM and PtLM in 1M H$_2$SO$_4$ and 2M methanol solution at a scan rate of 20 mV s^{-1} between 0 and 1.0 V vs SCE. Reprinted with permission from Ref. 159, Copyright 2011, American Chemical Society.

On the other hand, alloying of noble metals with one or more other elements such as Ru,[160] Mo,[161] Co,[120,162] Cu,[163] Zn,[122] Ir,[164] etc. supported on CNTs has been intensively studied to maximize the catalytic performance and minimize the costs. For instance, Hsieh et al. indicated that bimetallic PtZn alloy/MWNT synthesized by microwave-assisted polyol method was found to be a much better catalyst than Pt/MWNT for DMFCs.[122] This improvement can be linked to the bifunctional mechanism of the binary catalysts: the presence of Zn can promote the generation of Zn-OH species, thus more active Pt sites are available for reaction. In addition, our group found that the introduction of Co component into Pt/MWNT hybrids would also facilitate the electroactivity enhancement of methanol oxidation reaction.[162] When the atomic ratio of Pt/Co was 50:50, the PtCo/MWNT catalyst possessed the highest mass activity of 428.0 mA mg^{-1}, which was more competitive than Pt-MWNT (145.7 mA mg^{-1}) and commercial PtRu/Vulcan XC-72 catalyst (182.8 mA mg^{-1}). In another case, a multi-component composite of PbPtCu/CNT was reported as an efficient catalyst for electrooxidation of methanol.[163] The methanol oxidation peak current of this PbPtCu/CNT catalyst (94.4 mA cm^{-2}) was tested to be almost two times higher than that of the commercial PtRu/C (50 mA cm^{-2}).

3.1.5 Graphene

Graphene, a mono-layer graphite with a hexagonal packed lattice, has become the most intensively studied material since the first discovery in 2004.[165-168] In comparison with CNT, graphene has similar physicochemical properties but larger surface areas, which can be regarded as an unrolled SWNT.[169,170] From the viewpoint of fuel cell applications, graphene as a rising star has opened up a brand new avenue for designing the next generation catalysts, which are specifically expected to have increased electrocatalytic performance and enhanced antipoisoning ability.[2,171,172]

The most popular strategy for the fabrication of metal NPs/graphene composites can be summarized as follows: graphene oxide (GO) as a starting material is usually produced by exfoliation of graphite oxide obtained by the chemical treatment of natural graphite with strong oxidants, then the reduction of GO and loading of metal NPs could be achieved through different reduction processes, leading to the formation of metal NPs/graphene catalysts with diverse electrochemical performance.[123,173-178] Typically, Li's group prepared the composites of graphene nanosheets decorated with Pt nanoclusters via syn-reduction of GO and H$_2$PtCl$_6$ in the presence of NaBH$_4$.[173] Cyclic voltammogram experiments revealed that the peak current density on Pt/graphene coated electrode at the potential of 0.652 V (vs. Ag/AgCl) was 199.6 mA mg^{-1}, which was nearly twice of that on Pt/Vulcan (101.2 mA mg^{-1} at 0.664 V). Later, Li and co-workers described the use of ethylene glycol as an environmental friendly reductant to fabricate Pt NPs on graphene sheets.[174] Owning to the larger ECSA (36.3 m^2 g^{-1}) and better tolerance towards CO, the as-obtained Pt/graphene hybrid showed much more enhanced catalytic activity when compared with Pt/MWNT. Other similar examples of graphene-supported various alloy nanostructures, such as PtRu,[175,179-181] PtPd,[182,183] PtAu,[83] PtCo,[184,185] PtFe,[186,187] PtCu,[188] PtSn,[189] PdRu,[190] PdNi,[191] PtPdAu,[192] etc., prepared by using different metal precursor and reducing agents have also been reported and demonstrated improved electrocatalytic performance.

Since the functionality of graphene sheets has a great impact on the morphology and properties of supported active NPs, extensive efforts have been devoted to optimizing the graphene surface nature.[57,193,194] Kim et al. used thermal exfoliated-graphene nanosheets as highly functionalized materials for deposition of Pt NPs with high loading (40~80 wt%).[193] The mass activities of these Pt/graphene catalysts were at least twice as large as those observed with conventional Pt/C catalysts. In addition, the synthesis of the graphene-supported Pt or PtRu composites in a toluene and oleylamine medium resulted in a high dispersion of ultrafine Pt and PtRu NPs on carbon sheets,[195] which could help in maintaining the high active surface areas after several hours of catalyst use. Another effective modification is that Liu and co-workers decorated graphene sheets with CuPt alloy NPs with the aid of ionic liquid.[194] The presence of ionic liquid could not only preserve the intrinsic structures of graphene, but also increase the conductivity and avoid the aggregation of nanosheets, allowing CuPt/graphene catalyst to show much higher forward peak current density (780 mA mg^{-1}) than those of CuPt/C (275 mA mg^{-1}), Pt/graphene (329 mA mg^{-1}) and Pt/C (183 mA mg^{-1}) catalysts. Recently, our group employed low-defect graphene as an upgraded material for the preparation of advanced Pd/graphene electrocatalysts.[196] It is clearly seen from Fig. 12a that the charge transfer resistance in Pd/low-defect graphene (LDG/Pd) was much lower than that in Pd/RGO, Pd/MWNT and Pd/Vulcan XC-72 composites, which can be linked to the higher population of the triple-phase boundaries in the catalyst. In the presence of 0.5 M NaOH and 1 M methanol, the specific current density for Pd/low-defect graphene (27.6 mA cm^{-2}) was about 1.8~3.8 times those of the reference samples

(Fig. 12b), indicating it is a promising anode catalyst in DMFC applications.
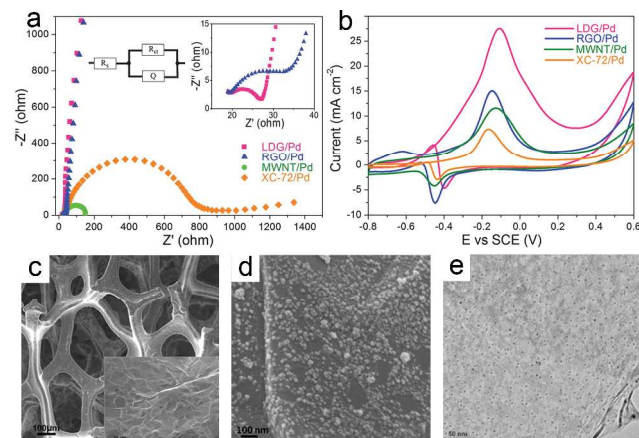
Fig. 12 (a) Nyquist plots of EIS for LDG/Pd, RGO/Pd, MWNT/Pd and XC-72/Pd at -0.2 V (vs. SCE) in 0.5 M NaOH with 1 M methanol. The insets are the equivalent circuit used to fit the impedance spectra (left) and local enlargement of the Nyquist plots for RGO/Pd and LDG/Pd (right). (b) CVs of LDG/Pd, RGO/Pd, MWNT/Pd and XC-72/Pd in 0.5 M NaOH with 1 M methanol at 50 mV s^{-1}. Reprinted with permission from Ref. 196, Copyright 2012, Royal Society of Chemistry. SEM images of the 3D graphene support (c) and Pt/3 D-GN catalyst (d). Inset in (c) is the enlarged picture. Reprinted with permission from Ref. 197, Copyright 2012, Royal Society of Chemistry. (e) TEM images of a Pt/3D-graphene composite by immobilization of 5 mL of (Pt)Ftn, the (Pt)Ftn concentration was 1.0 mM. Reprinted with permission from Ref. 198, Copyright 2013, American Chemical Society.

Furthermore, it has been reported that developing monolithic 3D network of graphene could extend its abilities towards fuel cell applications.[197,198] In a typical case from Maiyalagan et al.'s work.[197] the free-standing 3D graphene was first fabricated by chemical vapor deposition (CVD) using Ni foam as the template and ethanol as precursors, followed by the electrochemical deposition of Pt NPs with controllable morphology and size (Fig. 12c-d). Taking the advantages of interconnected seamless porous structure, high surface area and high electrical conductivity, the as-obtained Pt/3D graphene catalyst had high electrocatalytic activity (1.6 mA cm^{-2}) when compared with Pt/carbon fiber catalyst (0.8 mA cm^{-2}). This aspect was also demonstrated recently by Lim et al.,[198] who fabricated the Pt/3D graphene hybrid using ferritin protein nanocages as the template and examined its catalytic performance for methanol oxidation (Fig. 12e). The observed catalytic efficiency of Pt/3D graphene showed marked improvement over Pt/RGO and commercial Pt/C catalysts, which can be attributed to the concerted effect of the monodispersed Pt NPs and the 3D graphene with interconnected conductive network.

3.1.6 Other carbon materials

Besides the five frequently-used carbon supports discussed above, other non-mainstream carbon materials have also provided a great potential utilization in preparing composite catalysts.[199-201] Wei and co-workers studied Pt catalysts supported on carbon aerogel (CA) with different pore structures and a uniform Pt dispersion was achieved.[199] Their results showed the highest mass specific current for the methanol oxidation reaction on Pt/CA catalyst was 395.3 mA mg^{-1}, much higher than that on the E-TEK 20% Pt/C catalyst (118.4 mA mg^{-1}) under the same experimental

conditions. On the other hand, carbon paper (CP), a synthetic thin lightweight matrix with pore spaces on the micrometer scale, has also been regarded as an ideal conductive substrate for fuel cells.[202] Amini et al. exploited a series of bimetallic PtAu-coated carbon paper catalysts with varying Pt coverage by means of repeated Cu underpotential deposition (UPD) redox replacement procedure.[200] The highest Pt utilization efficiency for methanol oxidation reaction was observed on PtAu/CP catalyst with a thickness close to a monatomic Pt layer. Another interesting carbon support based on single-crystalline C_{60} was developed by Zhang et al.[201] Through the simple adjustment of the reaction parameters, different C_{60} nanostructures from hollow nanobowls, nanorings, or nanoplates to nanorods/nanowires could be selectively synthesized. After the subsequent loading of Pt, the onset potential of methanol oxidation for Pt/C_{60} nanobowls (0.10 V vs SCE) was found to be more negative than that for the Pt/C_{60}-solid-nanoball electrode (0.29 V vs SCE), which can be interpreted as being associated with the high surface-area-to-volume ratio of C_{60} hollow nanobowl (Fig. 13). Apart from the above, other carbon materials such as carbon nanocapsules,[203] carbon nanohorns,[204] etc. have also been explored as catalyst supports and displayed enhancements in electrochemical performance.
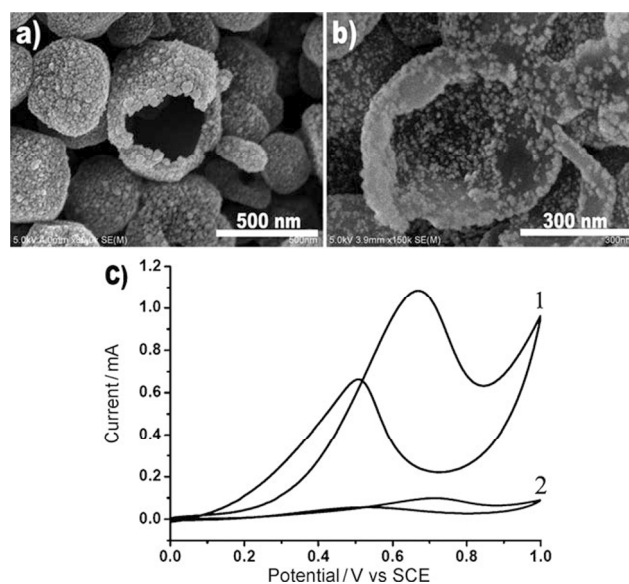
Fig. 13 SEM images of C_{60} hollow nanobowls deposited with Pt nanoparticles both outside (a) and inside (b). (c) Cyclic voltammograms of Pt/C_{60}-hollow-nanobowl (1) and Pt/C_{60}-solid-nanoball (2) electrodes in 2.0M methanol + 0.1M H_2SO_4. Scan rate: 30 mV s^{-1}. Reprinted with permission from Ref. 201, Copyright 2011, Wiley-VCH.

3.2 Multiple-carbon supported catalysts

As discussed above, each carbon material has its own advantages and disadvantages as DMFC catalyst support. Thus, it is difficult to obtain very satisfactory catalytic performance just by incorporation of metal NPs and a single-carbon support alone. In this regard, design and synthesis of multiple-carbon supports give a chance to simultaneously possess respective merits of each carbon material, which could meet the requirements of improving the electrocatalytic properties as well as cutting the costs.[205-214]

The typical route is to graft 1D carbon materials (e. g. CNTs) onto another carbon substrate, thus generating multiple-carbon

hybrids.[205-207] For example, a coral-like multiple-carbon material (Coral-C) has been synthesized by growing curled MWNTs onto carbon black (Lamp Black).[205] By combining the unique structures and properties of the two nanostructured carbons, the coral-like new carbon material offers the virtues of high electronic conductivity, chemical stability, and hydrophobicity, which could work as a preferable supporting material. As expected, the as-obtained Coral-C-supported Pt catalyst showed good catalytic activity and high power output in single DMFC, both of which preceded those for single-MWNT and single-carbon black supported catalysts. Later, Hsieh and co-workers used a catalytic CVD approach to synthesize CNTs directly grown on carbon paper.[206] In this hierarchy carbon-based composite, a large amount of CNTs could protrude out of the carbon paper and provide an external surface area for supporting Pt NPs with excellent electrochemical activity and durability (after a potential cycling of >1000 cycles). Similarly, a ternary composite of Pt/oxygen-incorporated bamboo-shaped CNTs-carbon cloth (Pt/O-BCNT/CC) was reported as an efficient catalyst for electrooxidation of methanol.[207] After 300 cycles, no significant change in the oxidation current density of Pt/O-BCNT/CC was observed.

In the past few years, graphene has become a hot topic of interest in fuel cell area. However, the electrical and mechanical properties of graphene would deteriorate when exfoliated graphene sheets horizontally restack via the Van der Waals forces and π-π interactions between the layers. This weakness necessitates the search for separation of graphene by embedding another carbon material that could prevent the carbon sheets from aggregates.[208,209] To achieve this goal, Han et al. fabricated graphene-carbon fiber mats by thermally treating electrospun polyacrylonitrile fibers decorated with GO.[208] In this case, the CNF surface became rough due to the presence of crinkly graphene and at the same time the graphene sheets were separated by the fibers, which were beneficial to the activity and long-term stability of the Pt NPs. More recently, Guo and co-workers used SiO₂-GO as the template and sucrose as the carbon precursor to prepare macroporous carbon–graphene composites by a casting method.[209] The insertion of macroporous carbon between graphene sheets effectively avoided the re-stacking of graphene, forming a hybrid carbon material simultaneously having the porous structure of macroporous carbon and the unique electrical and mechanical properties of graphene. After the subsequent loading of Pt NPs, the resulting electrocatalyst displayed an increased catalytic activity (81.6 mA mg^{-1}) toward the oxidation of methanol relative to Pt/graphene (34.7 mA mg^{-1}) and Pt/macroporous carbon (65.8 mA mg^{-1}) samples.

Recent results revealed that graphene and CNT can be a fairly good combination for the development of advanced DMFC electrocatalysts.[210-214] One representative contribution is that Ma et al. introduced long CNTs as nanospacers to bridge the adjacent graphene and inhibit the face-to-face aggregation of graphene sheets.[210] When used as a support for Pt NPs, the CNT/graphene architecture had synergistic effects on increasing the ECSA and the active sites of Pt because of its 3D graphitic, porous structure. Then, they reported the decoration of tiny and well-dispersed PtRu clusters onto such multiple-carbon substrate and indicated their improved electrocatalytic activity and CO-tolerance

ability.[211] Ramaprabhu's group performed a systematical investigation on the performance of PtRu NPs dispersed on the mixture of functionalized graphene (f-G) and functionalized MWNT (f-MWNT) in different ratios.[212] It was found that the optimum mass ratio of f-G/f-MWNT was 50:50 and a maximum power density of about 68 mW cm^{-2} could be obtained. Besides, a novel open-ended N-doped CNT–graphene hybrid nanostructure (NCNT-GHN) designed by Lv et al. should be highlighted.[213] Strikingly, fine PtRu NPs with diameters ranging from 2 to 4 nm could be immobilized onto these NCNT-GHN supports without using any pretreatment steps (Fig. 14a-c). Single-cell performance tests verified that the peak power density of PtRu/NCNT-GHN was much higher than those of commercial catalysts as well as PtRu/CNT (Fig. 14d), which was largely due to their unique hierarchical structure.
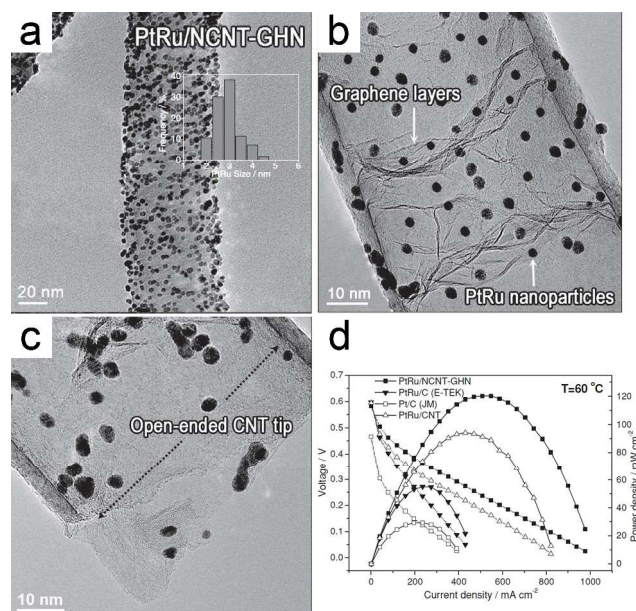
Fig. 14 Well-dispersed PtRu NPs on NCNT-GHN. Graphene layers inside the NCNTs can afford additional anchoring positions for PtRu NPs, in virtue of the open-ended tip structure of the NCNTs. The inset in (a) is the corresponding size-distribution histogram of the PtRu NPs in the PtRu/NCNT-GHN samples. Reprinted with permission from Ref. 213, Copyright 2011, Wiley-VCH.

3.3 Heteroatom-doped carbon supported catalysts

Heteroatom doping is an effective approach to tailor the properties of carbon materials and extend their potential applications in energy conversion devices.[215-217] Specifically, doping carbon nanostructures with heteroatoms such as nitrogen, boron, sulfur and etc. can substantially affect their electronic structures, chemical reactivity, pH as well as conductivity, and meanwhile keep the intrinsic physical/chemical characteristics well.[172,218] In addition to regulating the nature of carbon supports, the incorporation of heteroatoms is in favor of immobilization of active metal NPs, which is able to restrain their particle sizes and improve the electrochemical stability.[219,220] Therefore, such composites based on heteroatom-doped carbon have brought new design opportunities of high-performance anode catalysts.

3.3.1 Nitrogen-doped carbon
Among various heteroatoms, nitrogen atom is the most popular atomic specie used to dope the carbon framework of supporting

materials since its atomic radius is close to that of carbon atom.[221-223] Direct nitrogen-doping during the synthesis of carbon supports is a typical way for preparation of N-doped carbon structures.[224-230] For instance, Su et al. obtained N-doped porous carbon nanospheres (PCNs) via carbonizing polypyrrole nanospheres (PNs) followed by a chemical activation in the presence of KOH.[224] The presence of N atoms as localized defects could act as anchor sites and enable the formation of Pt NPs even dispersed on PCN surface. After comparative electrochemical measurements, the authors found that Pt/PCN had an enhanced MOR activity of 343 mA mg^{-1}, which was superior to Pt/carbon nanosphere (297 mA mg^{-1}) and commercial E-TEK catalyst (300 mA mg^{-1}). A copolymer, poly(1-butyl-3-vinylimidazolium bromide-co-acrylonitrile) (PBA), was also used as nitrogen/carbon source to yield nitrogen-doped carbon materials.[225] By changing the imidazolium ionic liquid molar ratio in the copolymers, the nitrogen contents and morphology of the resulting supporting materials could be conveniently tunable. As a result, Pt/nitrogen-doped carbon catalyst with a B/A molar ratio of 1:1 showed the relatively high oxidation mass peak current (103 mA mg^{-1}), mainly due to the synergistic effects between highly distributed Pt NPs and N-containing carbon matrix. Kuo's group successfully prepared N-doped porous carbon layer surrounding CNTs-supported Pt hybrid (Pt/NC-CNT) using aniline as a dispersant to separate the CNT bundles and the source of both carbon and nitrogen.[226] Especially, Pt NPs were well protected by being embedded inside the pores of N-doped carbon coating, resulting in a tremendously stable electrocatalytic activity. The decay in maximum current density for MOR was measured to be 20% for Pt/NC-CNT after 1000 cycles, which was obviously prior to Pt/C catalyst (76%). Later, the same group further investigated the effect of different carbonization temperatures on the structures and performance of aforementioned Pt/NC-CNT materials and documented that the most appropriate temperature was 600 °C.[227] To simplify the synthesis process and avoid using high-temperature condition, Sun and co-workers developed a low temperature (~160 °C) solvothermal route to synthesize nanoflower-like N-doped graphene by reaction of pentachloropyridine with potassium.[228] The as-prepared material was composed of sp^2-hybridized carbon and the designed nitrogen types (pyridine-like and quaternary nitrogen), which made the Pt NPs electrochemically more active in comparison to those supported on carbon black.

Besides direct N-doping routes, the formation of N-doped carbons can also be achieved by post-treatment of pre-synthesized carbon materials with nitrogen-containing precursor (e.g. N$_2$, NH$_3$ etc.).[218-220,231,232] Song et al. reported that N-doping in graphene sheets could be realized by the heat treatment of GO with NH$_3$ flow at various temperatures.[231] In these N-doped graphene materials, three types of nitrogen species including graphitic type, pyridine type and amino type were identified, and the latter two were proved to be better suited for uniform distribution of Pt NPs. The cyclic voltammetric tests for methanol oxidation indicated the Pt catalysts dispersed on N-doped graphene treated by annealing at 800°C had the highest activity of 135 mA mg^{-1}, not only due to the pyridinic nitrogen doped in the carbon network but also related to the enhanced conductivity. A more systematic investigation of the synthesis

conditions and parameters needed to prepare Pt loaded N-doped graphene hybrids was carried out by Zhou and co-workers.[219] TEM observations showed that both the annealing temperature and the reduction condition played key roles in size control of Pt NPs, which was essential for attaining exceptional catalytic performance. Zhu et al. developed an assembly strategy to disperse PtAu alloy NPs onto N-doped graphene sheets for the first time.[220] In this case, melamine was used as the nitrogen source to produce N-doped graphene materials and the catalytic properties of PtAu/N-doped graphene nanocomposite with a Pt/Au atomic ratio of 3:1 (417 mA mg^{-1}) were tested to be much better than the analogous undoped counterpart (186 mA mg^{-1}) and commercial Pt/C catalyst (64 mA mg^{-1}). Microwave-heating of the graphene in NH$_3$ atmosphere could also implement the nitrogen doping.[232] In this process, the reactants could absorb microwave easily thus reaching a high temperature (beyond 500°C) in few seconds. According to the half-cell electrochemical tests, the peak current density for the as-prepared Pt/N-doped graphene catalyst (24.9 mA cm^{-2}) was almost 2 times that for Pt/graphene (13.4 mA cm^{-2}).

To unravel the secret of the beneficial effects of nitrogen in carbon-supported catalysts, O'Hayre's group reported a direct observation of the nanoscale spatial correlation between nitrogen-containing regions and metal NPs on the surface of carbon support using an aberration-corrected scanning transmission electron microscope (STEM).[233] As seen from Fig. 15a-b, the greatest nitrogen modification took place at the edges of the graphitic carbon structure (area 1), and the lower concentration of nitrogen could be observed at regions more distant from the surface (area 2 and 3). Based on the analysis of overlay of the high angle annular dark-field (HAADF) and nitrogen map (Fig. 15c), the authors proposed a catalytic NPs-nitrogen defect interaction model: most metal NPs nucleated in regions with moderate nitrogen content, which are adjacent to the locations with the highest concentration of nitrogen (Fig. 15d). Then, they functionalized commercial catalysts with nitrogen and confirmed the improvements in performance and long-term durability.
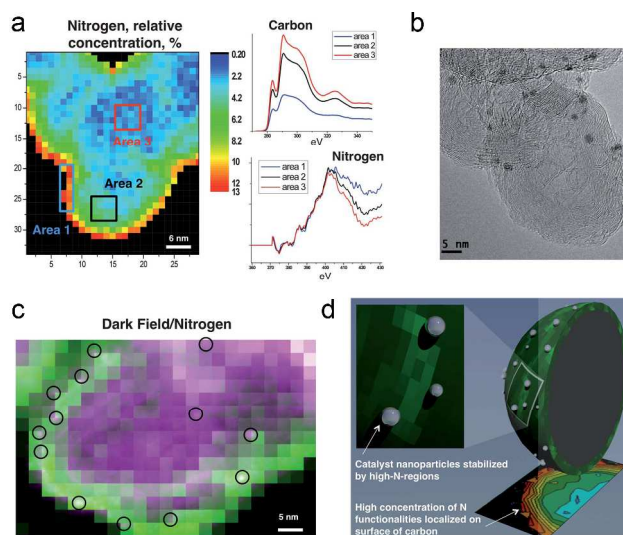
Fig. 15 (a) Nitrogen map showing relative concentration of nitrogen in different regions of graphitized carbon black particle, and C K-edge and N K-edge data from three areas highlighted on the map. (b) Typical HR-TEM image of Pt/Graphitic Vulcan. (c) Overlay of HAADF-STEM

(purple) and nitrogen EELS map (green) showing that metal NPs primarily nucleate in regions with moderate nitrogen content, which are adjacent to the locations with the highest level of nitrogen. (d) Schematic illustration of the catalyst nanoparticle–nitrogen defect interaction model developed from these investigations. Reprinted with permission from Ref. 233, Copyright 2013, Royal Society of Chemistry.

3.3.2 Other heteroatom-doped carbon

Boron and sulfur atoms have also been doped into various carbon materials to increase the chemical sensitivity of carbon surface.[234-237] Manthiram et al. synthesized B-doped CNTs by a CVD method using toluene and triethyl borate as the precursors for C and B.[234] Structural characterizations suggested that the existence of B atoms in the C lattices could boost the dispersion of Pt NPs, which would enlarge the electrochemical surface area and increase the Pt utilization efficiency. Not only that, the CO stripping voltammograms demonstrated the role of boron-doping to enhance the CO tolerance of Pt NPs, which can be explained in terms of the reasons that boron dopants absorbed more oxygen species, and therefore facilitated the removal of CO from the catalyst surface. Cabrera and co-workers described a field-enhanced diffusion with optical activation (FEDOA) technique to dope boron atoms into diamond particles without damaging their crystal structure.[235] The as-derived B-doped diamond NPs (BDDNP) was robust and chemically stable, which can be considered as a good carbon support for Pt and PtRu NPs. It can be drawn from the single fuel cell testing that the power density for the best PtRu/BDDNP system was up to 55 mW cm^{-2}, comparable to those obtained with amorphous carbon-supported catalytic systems. Although the introduction of both N and B atoms can help in optimizing the reactivity of precious metals, it should be noted that the detailed enhancement mechanisms of B-doping is different from that of N-doping. In the cases of Pt/B-doped carbon catalysts, the strong interaction between Pt NPs and B-doped carbon support is mainly due to a strong hybridization between platinum d orbitals and boron p orbitals, which means that the Pt atoms can be directly bonded to boron atoms.[221]

On the other hand, Amini's group described the synthesis of S-doped CNTs based on impregnation of CNTs with sulfur from toluene solution followed by a melt-coat step.[236] The study showed that the appropriate amount of sulfur modifier (S/CNT mass ratio of 0.3) afforded well-dispersed Pt NPs on CNTs with an average particle size of less than 3 nm, exhibiting a high mass-normalized methanol oxidation peak current of 862.8 mA mg^{-1}, which was ~6.5 folds of that for Pt/pristine CNTs (133.2 mA mg^{-1}) and ~2.3 folds of a commercial Pt/C (381.2 mA mg^{-1}). The virtues of S-doping have also been evident in using S-doped CNTs as a precursor for the synthesis of PtCo alloy catalysts.[237] Although the preparation process involved a high temperature annealing treatment, the presence of S component could prevent the sintering of alloy NPs and improve their electrochemical response for MOR.

Except for non-metallic heteroatoms discussed above, metal atoms-modified carbon-based catalysts have also been prepared by novel techniques and further used as anode materials for enhanced methanol oxidation reaction.[238] One important attempt for this aspect is that Sun and co-workers grew single-crystal Pt nanowires (NWs) over a coaxial nanocable support consisting of a tin NW and a carbon nanotube (Sn@CNT),[238] which was fabricated by a thermal evaporation method. Electron microscopy

observations displayed that the Sn@CNT support was composed of a Sn core and CNT shell with void space, and Pt NWs evenly anchored on Sn@CNT surface with lengths of up to hundred nanometers (Fig. 16a-c). Owning to the preferential exposure of certain crystal facets of the Pt NWs and the bi-functional mechanism between Pt and Sn, the electrode coated with 3D Pt NWs/Sn@CNT exhibited much lower peak potential (0.66 V) but higher mass activity (91.0 mA mg^{-1}) and I_f/I_b value (2.2) than those for Pt/C electrode (Fig. 16d).
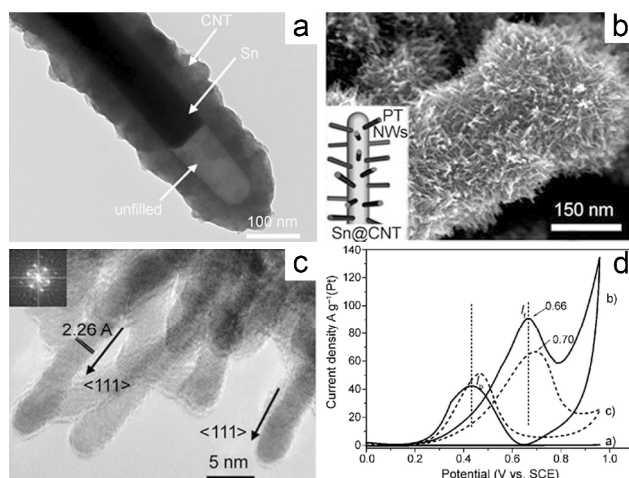
Fig. 16 (a) SEM image of pristine Sn@CNT nanocables, before the growth of Pt NWs. (b) HRSEM images of Pt NWs-Sn@CNT heterostructures. (c) HRTEM image of Pt NWs grown on Sn@CNT nanocables. (d) Cyclic voltammograms for methanol oxidation (1m methanol in 0.5m H$_2$SO$_4$). Trace a) before growth of Pt NWs; trace b) after growth of Pt NWs on Sn@CNT; trace c) ETEK commercial catalyst of Pt NPs on carbon black. Reprinted with permission from Ref. 238, Copyright 2010, Wiley-VCH.

3.4 Metal oxide-modified carbon supported catalysts

Metal oxide is another important promoter for DMFC catalysts that can provide hydroxyl sources at lower potentials and efficiently undergo a bi-functional mechanism.[14,239,240] Nevertheless, since most metal oxides deliver low specific surface areas and suffer from poor electron conductivity, it may be difficult to acquire adequate catalytic properties by the integration of noble metal NPs with metal oxide alone. In this background, people have been striving to exploit various metal oxides in combination with carbon to make better use of noble metals and lower the cost for the practicality of DMFCs. The following section will cover recent developments in applications of metal oxides-modified carbons as advanced anode supporting materials for DMFCs.

3.4.1 CeO$_2$

CeO$_2$ is normally employed as a co-catalyst in methanol electrooxidation due to its outstanding mechanical resistance, good anticorrosion ability, sizable surface defects as well as low price.[241-246] More importantly, as a fluorite oxide, CeO$_2$ is able to serve as an oxygen buffer to adjust surface oxygen content of the catalysts because the cation of CeO$_2$ can reversibly switch between the +3 and +4 oxidation states.[241-243] For example, Pt/CeO$_2$/C catalysts synthesized using a one-step reverse microemulsion method was proposed by Manthiram and co-workers.[241] In this case, Pt and CeO$_2$ NPs were homogeneously

deposited on the carbon support with an intimate contact between each other. This desired particle morphology could fully harness the enhancement effects of CeO₂, which was manifested in higher peak current density and durability than those for commercial Pt/C and PtRu/C. In 2011, Wang's group reported an important advance on novel structural design of Pt/CeO₂/C catalysts by anchoring the Pt NPs on mesoporous CeO₂ coated with amorphous carbon yielded by the β-cyclodextrin carbonization.[244] HRTEM images of Pt/CeO₂/C presented the crystal plane distance of Pt(111) and CeO₂(111), which could be further proved by the fast Fourier transform (FFT) patterns (Fig. 17a). This unique construction had successfully overcome the disadvantage from the poor electron conductivity of CeO₂, leading to a higher catalytic activity and stability toward methanol oxidation (Fig. 17b-c). Another ingenious approach for the synthesis of Pt/CeO₂/graphene hybrid was developed by Zhang et al.[245] In such a method, GO was used as a green oxidant to oxidize Ce^{3+} cations into CeO₂ NPs, while L-Lysine acted as linkers to connect Pt and CeO₂ NPs together on carbon sheets. As a result of synergies among Pt, CeO₂ and graphene, the newly designed catalyst showed evidently higher methanol oxidation current of 366 mA mg⁻¹ than those of simple Pt/graphene and commercial Pt/C catalysts. Moreover, the addition of shuttle-shaped CeO₂ with uniform crystalline orientation and smaller crystallite size into Pt/C systems was reported to gain more active sites and induce better Pt−CeO₂ interaction,[246] which in essence could highly promote electrochemical performance in terms of higher oxidation current and lower oxidation overpotential as compared with the bulk CeO₂. Other valuable contributions consist of a rapid sonication-facilitated deposition method for synthesis of PtRu/CeO₂/CNTs,[247] the investigation of the ceria promotion effect of Pt/CeO₂/C catalysts using HRTEM and EELS,[248] fabrication of PtRu/CeO₂/CNFs by an electrospinning technique[242] and a two-step synthetic route including hydrothermal and impregnation-chemical reduction method for Pt/CeO₂/graphene,[243] and all of them suggest the CeO₂-modified carbon materials have a splendid future as catalyst carriers in the field of electrocatalysis.
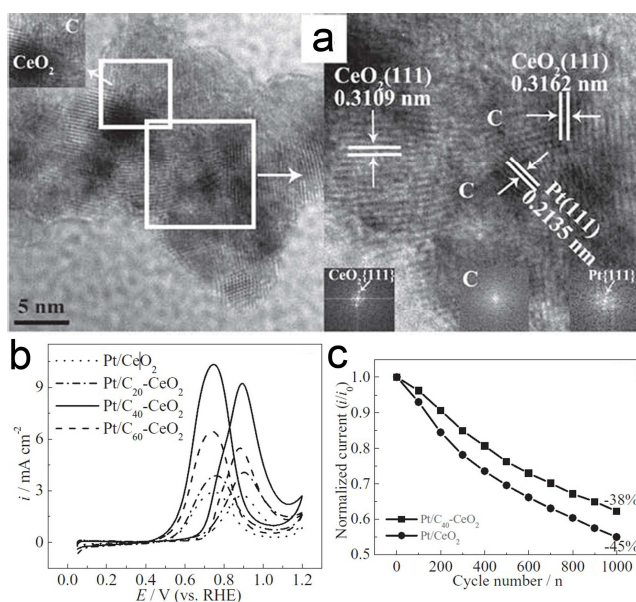
Fig. 17 (a) TEM images of Pt/C₄₀-CeO₂ catalyst (mesoporous CeO₂ coated with 40% carbon) and the HRTEM image acquired from the square region, which show the interplanar distance of Pt(111) and CeO₂(111). Insets show the FFT patterns, corresponding to the amorphous C, Pt(111), and CeO₂(111). (b) Cyclic voltammograms of methanol electro-oxidation on the Pt/CeO₂, Pt/C₂₀-CeO₂, Pt/C₄₀-CeO₂, and Pt/C₆₀-CeO₂ catalysts in an Ar-saturated solution of 0.5 mol L⁻¹ CH₃OH and 0.5 mol L⁻¹ H₂SO₄ at 25 ºC. Scanning rate: 0.05 V s⁻¹. (c) The normalized peak current plots of methanol electro-oxidation in an Ar-saturated solution of 0.5 mol L⁻¹ CH₃OH and 0.5 mol L⁻¹ H₂SO₄ at 25 ºC for the Pt/CeO₂ and Pt/C₄₀-CeO₂ catalysts. Reprinted with permission from Ref. 244, Copyright 2011, Wiley-VCH.

3.4.2 MnO₂

As is well known, MnO₂ has been realized as one of the most promising electrode materials for electrochemical supercapacitors.[249,250] In view of its attractive inherent properties, such as excellent proton conductivity, good chemical stability and environmental compatibility, MnO₂ is also a hopeful additive in DMFC anodic catalysts to improve the methanol electrooxidation kinetics.[251-256] Typically, Peng's group for the first time demonstrated the use of MnO₂-modified CNTs as a support in the preparation of novel Pt and PtRu catalysts.[251] During the catalytic reactions, the existence of MnO₂ could not only provide fast and barrier-free channels for electron and proton transfer, but also assist the removal of the poisoning intermediates from the Pt sites, enabling the hybrid catalysts to have higher electrochemical active surface area and better antipoisoning ability. By changing the deposition order of MnO₂ and PtRu NPs on CNTs, the surface of PtRu/CNT composites could be covered by MnO₂, which was capable of preventing the dissolution of PtRu NPs as well as the corrosion of the CNTs, and thus insuring more stable performance.[252] Additionally, the enhancement function of MnO₂ component is also reflected in catalyzing methanol oxidation in alkaline media.[253,254] For example, Zhao et al. reported the fabrication of a ternary Pd/MnO₂/CNT electrocatalyst that exhibited higher specific activity (431.0 mA mg⁻¹) in 0.5 M NaOH solution with 1 M methanol.[253] Analogously, the composites of Pd/MnO₂/graphene have also been synthesized and tested to be efficient catalysts for alkaline DMFCs.[254] Furthermore, it should be emphasized that the electrochemical activity of MnO₂ largely depends on its microstructure and morphology.[257,258] On this front, our group succeeded in constructing a sophisticated hybrid composed of Pt NPs, graphene and birnessite-type MnO₂ nanolamellas (MNLs) by utilizing GO as a green reducing agent, as depicted in Fig. 18a.[255] It is striking that extremely small Pt NPs with an average diameter of only 1.7 nm were formed and uniformly dispersed on MNL/graphene sheets, which was partially attributed to the extra merits of MNLs such as high surface area, low density, and good permeation (Fig. 18b-c). As a consequence, the as-derived Pt/MNL/graphene architecture expressed ultrahigh forward anodic peak current density (1224 mA mg⁻¹), notably superior to Pt/graphene (357 mA mg⁻¹), Pt/C (225 mA mg⁻¹) and Pt/MnO₂/C (435 mA mg⁻¹) samples (Fig. 18d). The deposition of Pd NPs on above MNL/graphene was also achieved by a similar procedure and the composite was evaluated to be an active electrocatalyst for methanol oxidation in alkaline solution.[256]
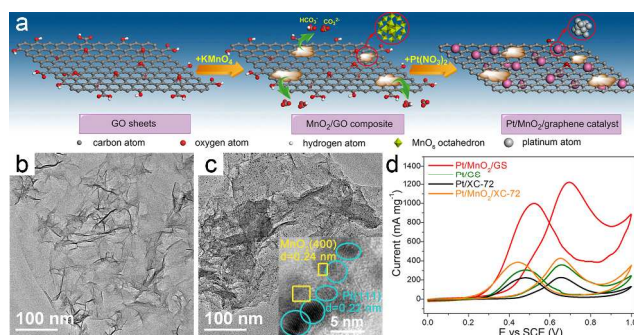
Fig. 18 (a) Illustrations of the synthesis of Pt/MnO2/graphene catalyst. TEM images of MnO2/GO (b) and Pt/MnO2/GS (c). The inset of (c) is an HRTEM image of Pt/MnO2/GS. (d) CVs of Pt/MnO2/GS, Pt/GS, Pt/XC-
5 72 and Pt/MnO2/XC-72 in 1 M H2SO4 and 2 M methanol at 20 mV s^{-1}. Reprinted with permission from Ref. 255, Copyright 2013, Elsevier B.V.

3.4.3 TiO$_2$

TiO$_2$ can be conceived as an attractive support because of its stability in fuel cell working atmospheres, semiconductivity,
10 natural abundance and relative nontoxicity.[259-262] Moreover, theoretical calculations demonstrated that TiO$_2$ could weaken the Pt-CO bonding and lower CO activation energy for surface mobility, leading to a more facile diffusion of CO from Pt sites.[263,264] For instance, Pt/TiO$_2$/carbon arrays have been
15 successfully prepared by using TiO$_2$ nanotube as a highly orientated and uniform template.[259] The modification of graphitized carbon significantly enhanced the conductivity of TiO$_2$ and thus reached its full potential, which could speed up the removal of the byproduct CO-like species. Another typical case is
20 that Sugimoto et al. thoroughly mixed TiO$_2$ nanosheets derived from layered H$_2$Ti$_4$O$_9$ with PtRu/C to obtain a composite catalyst.[260] With a low TiO$_2$ content, an increase in the electrochemically active PtRu surface area and methanol oxidation activity could be observed, resulting from the increased
25 interphase between the electrolyte and PtRu NPs because of the hydrophobic nature of TiO$_2$ nanosheets. Lou's group reported the formation of 3-component Pt/TiO$_2$/RGO junctions by a facile hydrothermal method.[261] In this work, Pt NPs were exclusively anchored at the interface between TiO$_2$ and RGO, generating
30 sufficient 3-phase interface. Electrochemical measurements showed that the activity of the Pt/TiO$_2$/RGO electrocatalyst (83.1 mA cm^{-2}) was 1.81 times higher than that of Pt/RGO sample (45.8 mA cm^{-2}). Most recently, PtNi alloy NPs have been loaded on carbon-doped TiO$_2$ nanotube arrays and successfully applied
35 as anode catalysts for photo-assisted methanol oxidation.[262] Under illumination, the photo-induced electron–hole pairs were produced on the surface of TiO$_2$, and the latter could directly oxidize methanol as well as the intermediates, finally obtaining a significant pickup in catalytic activity. In addition to the results
40 noted above, several groups have designed some other techniques for preparing high-performance TiO$_2$/carbon-based catalysts toward the electrocatalytic oxidation of methanol, such as sandwich-structured Pt/TiO$_2$/graphene hybrid,[265] Pt/TiO$_2$/C composite with hetero interfaces,[266] TiO$_2$-embedded CNFs
45 decorated by PtRu NPs[264] and ultra-long Pt nanolawns supported on TiO$_2$-coated CNFs,[267] etc.

3.4.4 Other metal oxides

Other metal oxides have also been reported as alternative activators in creating multi-component catalysts with improved

50 catalytic ability.[268-273] Rao and co-workers incorporated MoO$_3$ on Vulcan XC-72 through an intermittent microwave heating (IMH) method, and subsequently dispersed small Pt NPs over the MoO$_3$/C surface.[268] Surprisingly, the non-conducting MoO$_3$ was able to be electrochemically reduced to a conductive hydrogen
55 molybdenum bronze (H$_x$MoO$_3$) in acidic solution, which could function as a proton acceptor to accelerate the conversion of adsorbed intermediates to carbon dioxide and thus keep the Pt electrode surface clean. Accordingly, the peak current for methanol oxidation on Pt/MoO$_3$/C electrode was found to be
60 about 128% higher than that on PtRu/C electrode. In another case, a ternary Pt/CuO/C catalyst was obtained by a microwave irradiation method,[269] which ensured the miniaturization and effective dispersion of Pt NPs. The electrode made of such hybrid possessed a low degree of surface poisoning, hence exhibiting a
65 high I$_F$/I$_R$ value of 3.2. Yang et al. demonstrated that the introduction of Mn$_3$O$_4$ into the Pt/MWNT composites tended to decrease the average diameter of Pt crystal from 3.3 to 2.6 nm.[270] Cyclic voltammogram and chronoamperometric studies further showed an apparent promoting effect of Mn$_3$O$_4$ in both activity
70 and stability of Pt/MWNT sample. This finding has also been confirmed by Ye and co-workers' study.[271] They made a meticulous comparison with electrochemical stability of different metal oxides (CeO$_2$, NiO, Co$_3$O$_4$ and Mn$_3$O$_4$)-promoted Pd/C electrocatalysts and found that Pd/Mn$_3$O$_4$/C gave the best steady-
75 state performance in alkaline medium. More recently, ordered mesoporous carbons doped with tungsten oxide hybrids (WO$_3$/OMC) were obtained by thermal decomposition of phosphotungstic acid on OMC surface in N$_2$ atmosphere.[272] Given the appealing properties such as high specific surface
80 areas, good electronic conductivity and large pore volumes, the as-made WO$_3$/OMC composite was an appropriate candidate as supporting material of Pt NPs. During the electrochemical tests, the mass-specific activity towards MOR of Pt/WO$_3$/OMC electrocatalyst (410 mA mg^{-1}) prepared at appropriate
85 temperature far exceeded those of commercial Pt/C catalyst (171 mA mg^{-1}) and reference catalyst without WO$_3$ (168 mA mg^{-1}). Kurungot et al. has explored a novel strategy to effectively tune the functionality of Pt/RuO$_2$/CNF systems from charge storage to electrocatalysis.[273] Amazingly, random deposition of Pt and RuO$_2$
90 NPs on pristine CNFs resulted in the formation of a ternary composite rich in RuO$_2$ characteristics, while the use of H$_2$O$_2$-treated CNFs could obtain a material rich in Pt features on the surface. The former displayed typical charge storage properties of hydrous RuO$_2$, whereas the latter showed distinct electrocatalytic
95 behavior with respect to methanol oxidation. Besides, a number of new interesting results based on SnO$_2$,[274] ZnO,[115] Nb$_2$O$_5$,[275] etc. promoted carbon catalysts for methanol oxidation have also been reported and exhibited impressive catalytic abilities.

3.5 Polymer-modified carbon supported catalysts

100 Over the last several years, a considerable part of the studies on developing highly active DMFC anode catalysts have focused on the functionalization of carbon materials with various polymers. On the whole, there are two primary types of polymers commonly used in hybrid electrode materials: one is conducting
105 polymer, and another is polyelectrolyte. As we mentioned above, each of them has a helpful effect on manipulating the growth of metal NPs, which is critical to give full play to their catalytic

functions.

3.5.1 Conducting polymers

Conducting polymer nanostructures as promising reinforcers in electrode catalysts have received special attention due to their highly π-conjugated polymeric chains, low resistance, reversible doping/de-doping process, and controllable chemical and electrochemical properties.[62,276,277] For instance, polyaniline (PANI) is one of the most representative conducting polymers used for building up novel hybrid catalysts with hierarchical structures.[61,62,65,68,69] Mu and co-workers reported a notable method for the synthesis of Pt/PANI/CNT,[61] where PANI established a bridge connecting Pt NPs and CNTs. As shown in Fig. 19a-c, the conjugated PANI could interact with π-bond of CNTs via π-stacking without damaging the CNT framework, and simultaneously the covalent bonding between the Pt atoms and N atoms in PANI guaranteed the strong adherence of Pt NPs to CNT surface. Remarkably enough, Pt/PANI/CNT experienced 4500 cycles before ECSA drops to 40% of the initial value, which was more durable than Pt/C (1400 cycles) and Pt/CNT (3100 cycles) (Fig. 19d-e). Later, an interfacial polymerization method was developed to fabricate high-quality PANI-wrapped CNTs with core–shell heterostructure,[62] which could work as an efficient adsorbent for metal NPs. After forming Pt/PANI/CNT composite, the ECSA and I_F/I_R values were able to reach 110.2 $m^2 g^{-1}$ and 1.62, respectively, which met the requirements of both exceptional electrocatalytic activity and high tolerance toward CO poisoning. Huang et al. successfully assembled Pt NPs onto PANI-functionalized graphite nanoplatelet (GNP) via a solution blending method.[69] With a moderate amount of PANI (2 wt%), the Pt/PANI/GNP composite displayed the highest mass catalytic activity, about two times higher than that of Pt/GNP catalyst.
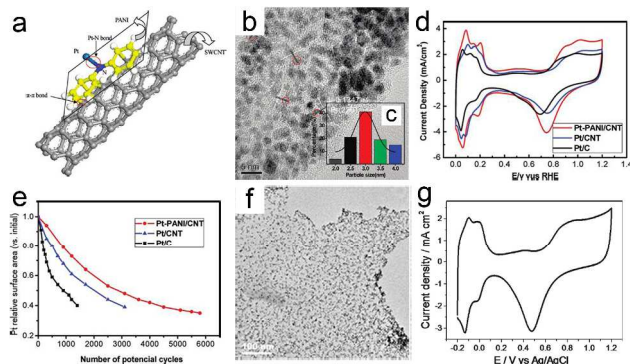
Fig. 19 (a) Molecular interactions in the synthesized Pt-PANI/CNT catalyst. HRTEM image of the Pt-PANI/CNT catalysts (b), and size distribution of Pt nanoparticles on the CNTs (c). (d) CV curves of Pt-PANI/CNT, Pt/CNT, and Pt/C catalysts. Reprinted with permission from Ref. 61, Copyright 2011, American Chemical Society. (e) ECSA of the catalysts as a function of the number of potential cycles. (f) TEM image of the Pt/graphene catalysts with Pt loading of 50 wt %. (g) CV of the Pt/graphene (Pt loading 60 wt%) catalysts modified glassy carbon electrode in a N_2-saturated 0.5 M H_2SO_4 solution at a scan rate of 50 mV s^{-1}. Reprinted with permission from Ref. 72, Copyright 2011, American Chemical Society.

Other conducting polymers have also been studied for hybrid anode systems.[63,86,278] Zhao et al. demonstrated the feasibility of polypyrrole (PPY)-functionalized graphene as a new supporting material for DMFC application.[63] Similar to PANI-functionalized carbon supports, the PPY/graphene could increase the rate of charge transfer and provide more active area for Pd dispersing. As compared with Pd/graphene (265.8 mA mg^{-1}) and Pd/C (205.3 mA mg^{-1}), the Pd/PPY/graphene nanocomposite delivered a high peak current density of 359.8 mA mg^{-1} with an improved stability. He and co-workers coated a conducting poly(2-amino-5-mercapto-1,3,4- thiadiazole) (PAMT) film on solid carbon paste (SCP) to form an attractive hybrid support of Pt electrocatalysts.[278] Interestingly, relatively small Pt NPs decorated on PAMT/SCP showed a chestnut bur-like morphology with numerous nanothorns, which was advantageous to exert their catalytic activity because of the abundant active sites. Voltammetric data indicated that the integration of PAMT with SCP contributed to increase the ECSA of Pt catalysts and therefore positively impact the electrocatalytic performance. Another intriguing work was performed by Mu et al.[86] Graphene was utilized as a catalyst for the electrochemical oxidative polymerization of pyrogallol, then the resulting poly(pyrogallol) (PPG)/graphene composite was available as a superior platform for suppressing the agglomeration of Pt particles due to the presence of plentiful oxygen-containing functional groups. The activity studies employing cyclic voltammetry and chronoamperometry techniques illustrated that a pronounced increase in anodic peak current density and a less susceptibility to CO poisoning were obtained on Pt/PPG/graphene electrode.

3.5.2 Polyelectrolyte

Numerous investigations suggest that modifying carbon materials with polyelectrolyte is a practical way to produce highly dense and homogeneously distributed metal NPs as well as avoid damaging the electronic network of carbon supports, which are very meaningful to the electrocatalytic-related applications.[71-74,279,280] A typical example of this is that Qiu et al. demonstrated Pt NPs assembled on PDDA-functionalized graphene sheets,[72] as seen in Fig. 19f. The resultant Pt/PDDA/graphene nanocomposite showed ultrahigh electrochemical active surface area of up to 141.6 $m^2 g^{-1}$ (Fig. 19g), implying a high utilization of Pt in the hybrid under the assistance of PDDA. Aiming at further enhancing the catalytic activity and the resistance to CO poisoning, the adjustment of Pt loadings on PDDA/graphene surface have been conducted by Yan and co-workers.[71] With a mass ratio between Pt and PDDA/graphene of 80%, the as-prepared composite exhibited ~150% and ~60% enhancements in current density and I_F/I_R value compared to Pt/PDDA/C sample, respectively. Chitosan (CS) and heteropolyacids (HPAs) of $H_3PMo_{12}O_{40}$ and $H_3PW_{12}O_{40}$ were also adopted to functionalize CNTs.[279] In acid solutions, the protonation of the amino groups could make CS a cationic polyelectrolyte, and thus provide a suitable microenvironment for the accommodation of anion catalytic center of HPAs, which not only inhibited the aggregation of PtRu NPs but also improved their activity. Electrochemistry analyses showed that the PtRu/HPA-CS/CNT catalysts afforded highly boosted electrocatalytic properties, significantly surpassing the PtRu/acid-treated CNT catalysts. In another case, Imae et al. used cationic poly(amido amine) (PAMAM) dendrimers (DENs) as protectors and binders to immobilize Pt NPs onto the external walls of CNTs.[280] As a consequence of mutual effects among Pt, PAMAM and CNTs, low anodic potentials at around 0.38–0.58 V in the forward scan and high I_F/I_R values of 2.3-8.1 were both achieved, indicatives of the easy occurrence of methanol oxidation reaction and almost

complete oxidation of methanol to CO_2, respectively.

4. Conclusion, challenges and perspective

As the most important catalyst supports for fuel cells, carbon materials and their derivatives can be incorporated with various active metal (mainly noble metal) NPs to improve the catalytic performance and lower the manufacturing cost due to their attractive features such as natural abundance, processability, high surface area, excellent electrical conductivity and environmentally friendly. However, carbon supports are relatively easy to be corroded under harsh fuel cell operation conditions, which would cause a rapid decay of electrochemical performance. To circumvent this shortcoming, the rational construction of carbon-based electrode materials with more advanced architectural design has been identified as the major solution. In the last three years, a great number of exciting research achievements on novel carbon-based anode catalysts for DMFCs have been made. Herein, we have systematically reviewed recent important progress in this hot field. Specifically, diverse advanced strategies and techniques for the fabrication of carbon-based anode electrocatalysts with different compositions, architectures and morphologies, as well as the utilization of these hybrid catalysts toward methanol oxidation reactions are covered.

Although the developments of newly designed carbon-based anode catalysts hold out a tempting prospect in addressing the energy and environmental issues, much more remains to be done, when considering to make them commercially viable. At present, there are at least four major challenges. The first is that it is extremely difficult to balance the contradictions between modification of carbon materials with functional groups and protection of their intrinsic structures and properties. A higher surface-functionalization level of carbon materials undoubtedly makes them more vulnerable to be excessively oxidized, even resulting in a structural collapse. Given this, it necessarily deserves the exploration of rational synthesis methods to open up the possibility of introducing anchor sites on carbon surface without affecting the original electronic network. Second, the electrocatalytic activity of carbon-based anode materials is limited by the size, shape, microstructure and dispersion of supported active metal NPs. Unfortunately, the formation processes of metal NPs on carbon substrate are not fully understood, and at present, well controlling their growth is a bottleneck in achieving satisfactory catalytic ability. Therefore, a more careful and sophisticated manipulation of monodisperse, ultrafine metal NPs with rich high-index facets and a much stronger interaction between NPs and carbon supports are highly desired. Third, the underlying mechanisms of enhancement in catalytic activity by carbon-based composites are partly unclear. For example, the relationship between electrochemical performance and carbon content in the hybrids is controversial. Thus, more studies remain to be done in disclosing the real functions of various carbon components for catalyzing methanol oxidation. Finally, there is lacking of cost-effective and environmentally friendly approaches for the large-scale production of high-quality carbon materials (especially for nanostructured carbons such as C_{60}, CNT and graphene etc.) with high purity, tunable sizes and low defect density. At this point, extensive multidisciplinary collaboration among physicists, chemists, biologists and materials scientists may provide some fresh ideas and opportunities.

Despite these obstacles, it is great to see that the keen interest and the high attention degree in anode catalysts have not faded, with a growing number of new researchers devoted to this area. Within this context, we believe that the rapid development of carbon-based hybrid materials will fuel up the accessing of next generation renewable electronic devices equipped with high-performance DMFC energy systems, which is expected to not only bring a great convenience to our daily life but also have enormously beneficial effects on natural environment. Overall, the opportunities and challenges that rest on these interesting targets should attract the continuous efforts of many scientists and engineers in this important and fantastic area.

Acknowledgment

Notes and references

Key Laboratory of Soft Chemistry and Functional Materials (Nanjing University of Science and Technology), Ministry of Education, Nanjing, 210094, China. Fax: +86-25-8431-5054; Tel: +86-25-8430-5667; E-mail: wangx@mail.njust.edu.cn
†Dedicated to Professor Xinquan Xin on the occasion of his 80th birthday.

1. S. Chu and A. Majumdar, *Nature*, 2012, **488**, 294-303.
2. N. G. Sahoo, Y. Pan, L. Li and S. H. Chan, *Adv. Mater.*, 2012, **24**, 4203-4210.
3. A. L. M. Reddy, S. R. Gowda, M. M. Shaijumon and P. M. Ajayan, *Adv. Mater.*, 2012, **24**, 5045-5064.
4. H. Wang and H. Dai, *Chem. Soc. Rev.*, 2013, **42**, 3088-3113.
5. B. C. H. Steele and A. Heinzel, *Nature*, 2001, **414**, 345-352.
6. M. Winter and R. J. Brodd, *Chem. Rev.*, 2004, **104**, 4245-4270.
7. Y.-G. Guo, J.-S. Hu and L.-J. Wan, *Adv. Mater.*, 2008, **20**, 2878-2887.
8. N.-S. Choi, Z. Chen, S. A. Freunberger, X. Ji, Y.-K. Sun, K. Amine, G. Yushin, L. F. Nazar, J. Cho and P. G. Bruce, *Angew. Chem. Int. Ed.*, 2012, **51**, 9994-10024.
9. A. S. Aricò, S. Srinivasan and V. Antonucci, *Fuel Cells*, 2001, **1**, 133-161.
10. Y. Paik, S.-S. Kim and O. H. Han, *Angew. Chem. Int. Ed.*, 2008, **47**, 94-96.
11. Z. Wen, J. Liu and J. Li, *Adv. Mater.*, 2008, **20**, 743-747.
12. E. Antolini, *Energy Environ. Sci.*, 2009, **2**, 915-931.
13. C. Koenigsmann and S. S. Wong, *Energy Environ. Sci.*, 2011, **4**, 1161-1176.
14. L. Cao, F. Scheiba, C. Roth, F. Schweiger, C. Cremers, U. Stimming, H. Fuess, L. Chen, W. Zhu and X. Qiu, *Angew. Chem. Int. Ed.*, 2006, **45**, 5315-5319.
15. E. Reddington, A. Sapienza, B. Gurau, R. Viswanathan, S. Sarangapani, E. S. Smotkin and T. E. Mallouk, *Science*, 1998, **280**, 1735-1737.
16. Y. H. Lin, X. L. Cui, C. H. Yen and C. M. Wai, *Langmuir*, 2005, **21**, 11474-11479.
17. X. Zhao, M. Yin, L. Ma, L. Liang, C. Liu, J. Liao, T. Lu and W. Xing, *Energy Environ. Sci.*, 2011, **4**, 2736-2753.
18. A. Halder, S. Sharma, M. S. Hegde and N. Ravishankar, *J. Phys. Chem. C*, 2009, **113**, 1466-1473.
19. Y. Kang, J. B. Pyo, X. Ye, T. R. Gordon and C. B. Murray, *Acs Nano*, 2012, **6**, 5642-5647.
20. S. Sharma and B. G. Pollet, *J. Power Sources*, 2012, **208**, 96-119.

21. S. Basri, S. K. Kamarudin, W. R. W. Daud and Z. Yaakub, *Int. J. Hydrogen Energy*, 2010, **35**, 7957-7970.

22. E. Frackowiak and F. Béguin, *Carbon*, 2001, **39**, 937-950.

23. H. S. Liu, C. J. Song, L. Zhang, J. J. Zhang, H. J. Wang and D. P. Wilkinson, *J. Power Sources*, 2006, **155**, 95-110.

24. L. Dai, D. W. Chang, J.-B. Baek and W. Lu, *Small*, 2012, **8**, 1122-1122.

25. D. S. Su, S. Perathoner and G. Centi, *Chem. Rev.*, 2013, **113**, 5782-5816.

26. D. Jariwala, V. K. Sangwan, L. J. Lauhon, T. J. Marks and M. C. Hersam, *Chem. Soc. Rev.*, 2013, **42**, 2824-2860.

27. H. Chu, L. Wei, R. Cui, J. Wang and Y. Li, *Coord. Chem. Rev.*, 2010, **254**, 1117-1134.

28. B. Wu, Y. Kuang, X. Zhang and J. Chen, *Nano Today*, 2011, **6**, 75-90.

29. J. J. Wang, G. P. Yin, J. Zhang, Z. B. Wang and Y. Z. Gao, *Electrochim. Acta*, 2007, **52**, 7042-7050.

30. A. Leela Mohana Reddy and S. Ramaprabhu, *J. Phys. Chem. C*, 2007, **111**, 16138-16146.

31. D. Sebastián, J. C. Calderón, J. A. González-Expósito, E. Pastor, M. V. Martínez-Huerta, I. Suelves, R. Moliner and M. J. Lázaro, *Int. J. Hydrogen Energy*, 2010, **35**, 9934-9942.

32. J. Guo, G. Sun, Q. Wang, G. Wang, Z. Zhou, S. Tang, L. Jiang, B. Zhou and Q. Xin, *Carbon*, 2006, **44**, 152-157.

33. C. Xu, X. Wang and J. W. Zhu, *J. Phys. Chem. C*, 2008, **112**, 19841-19845.

34. B. Seger and P. V. Kamat, *J. Phys. Chem. C*, 2009, **113**, 7990-7995.

35. J. H. Bang, K. Han, S. E. Skrabalak, H. Kim and K. S. Suslick, *J. Phys. Chem. C*, 2007, **111**, 10959-10964.

36. D. Wang, Y. Liu, J. Huang and T. You, *J. Colloid Interface Sci.*, 2012, **367**, 199-203.

37. N. Muthuswamy, J. L. G. de la Fuente, P. Ochal, R. Giri, S. Raaen, S. Sunde, M. Ronning and D. Chen, *Phys. Chem. Chem. Phys.*, 2013, **15**, 3803-3813.

38. P. Hernández-Fernández, S. Baranton, S. Rojas, P. Ocón, J.-M. Léger and J. L. G. Fierro, *Langmuir*, 2011, **27**, 9621-9629.

39. Y. L. Hsin, K. C. Hwang and C. T. Yeh, *J. Am. Chem. Soc.*, 2007, **129**, 9999-10010.

40. Y. Y. Mu, H. P. Liang, J. S. Hu, L. Jiang and L. J. Wan, *J. Phys. Chem. B*, 2005, **109**, 22212-22216.

41. S. J. Guo, S. J. Dong and E. K. Wang, *Adv. Mater.*, 2010, **22**, 1269-1272.

42. S. Chen, Z. Wei, L. Guo, W. Ding, L. Dong, P. Shen, X. Qi and L. Li, *Chem. Commun.*, 2011, **47**, 10984-10986.

43. Y. Hernandez, V. Nicolosi, M. Lotya, F. M. Blighe, Z. Y. Sun, S. De, I. T. McGovern, B. Holland, M. Byrne, Y. K. Gun'ko, J. J. Boland, P. Niraj, G. Duesberg, S. Krishnamurthy, R. Goodhue, J. Hutchison, V. Scardaci, A. C. Ferrari and J. N. Coleman, *Nat. Nanotechnol.*, 2008, **3**, 563-568.

44. C.-H. Hsu, H.-Y. Liao and P.-L. Kuo, *J. Phys. Chem. C*, 2010, **114**, 7933-7939.

45. A. Bagri, C. Mattevi, M. Acik, Y. J. Chabal, M. Chhowalla and V. B. Shenoy, *Nat. Chem.*, 2010, **2**, 581-587.

46. Y. Y. Shao, S. Zhang, C. M. Wang, Z. M. Nie, J. Liu, Y. Wang and Y. H. Lin, *J. Power Sources*, 2010, **195**, 4600-4605.

47. H. Huang, H. Chen, D. Sun and X. Wang, *J. Power Sources*, 2012, **204**, 46-52.

48. W. Qian, R. Hao, J. Zhou, M. Eastman, B. A. Manhat, Q. Sun, A. M. Goforth and J. Jiao, *Carbon*, 2013, **52**, 595-604.

49. D. Tasis, N. Tagmatarchis, A. Bianco and M. Prato, *Chem. Rev.*, 2006, **106**, 1105-1136.

50. V. Georgakilas, D. Gournis, V. Tzitzios, L. Pasquato, D. M. Guldi and M. Prato, *J. Mater. Chem.*, 2007, **17**, 2679-2694.

51. K. P. Loh, Q. Bao, P. K. Ang and J. Yang, *J. Mater. Chem.*, 2010, **20**, 2277-2289.

52. H. Chu, Y. Shen, L. Lin, X. Qin, G. Feng, Z. Lin, J. Wang, H. Liu and Y. Li, *Adv. Funct. Mater.*, 2010, **20**, 3747-3752.

53. C.-H. Hsu, H.-Y. Liao, Y.-F. Wu and P.-L. Kuo, *Acs Appl. Mater. Interfaces*, 2011, **3**, 2169-2172.

54. L. Li, J. Zhang, Y. Liu, W. Zhang, H. Yang, J. Chen and Q. Xu, *ACS Sustainable Chem. Eng.*, 2013, **1**, 527-533.

55. D. Wang, S. Lu and S. P. Jiang, *Electrochim. Acta*, 2010, **55**, 2964-2971.

56. Y. Zhao, X. Yang, J. Tian, F. Wang and L. Zhan, *Mater. Sci. Eng. B*, 2010, **171**, 109-115.

57. W. Xiao, Z. Sun, S. Chen, H. Zhang, Y. Zhao, C. Huang and Z. Liu, *RSC Advances*, 2012, **2**, 8189-8193.

58. H. Ming, X. Li, Y. Wei, L. Bu, Z. Kang and J. Zheng, *RSC Advances*, 2013, **3**, 3655-3660.

59. S. Guo, S. Dong and E. Wang, *Acs Nano*, 2010, **4**, 547-555.

60. J. Liu, S. Fu, B. Yuan, Y. Li and Z. Deng, *J. Am. Chem. Soc.*, 2010, **132**, 7279-7281.

61. D. He, C. Zeng, C. Xu, N. Cheng, H. Li, S. Mu and M. Pan, *Langmuir*, 2011, **27**, 5582-5588.

62. L. Shi, R.-P. Liang and J.-D. Qiu, *J. Mater. Chem.*, 2012, **22**, 17196-17203.

63. Y. Zhao, L. Zhan, J. Tian, S. Nie and Z. Ning, *Electrochim. Acta*, 2011, **56**, 1967-1972.

64. J. Zong, Q. Jin and C. Huang, *J. Solid State Electrochem.*, 2013, **17**, 1339-1348.

65. B. Qu, Y. Xu, Y. Deng, X. Peng, J. Chen and L. Dai, *J. Appl. Polym. Sci.*, 2010, **118**, 2034-2042.

66. X.-C. Liu, G.-C. Wang, R.-P. Liang, L. Shi and J.-D. Qiu, *J. Mater. Chem. A*, 2013, **1**, 3945-3953.

67. R. Yue, Q. Zhang, C. Wang, Y. Du, P. Yang and J. Xu, *Electrochim. Acta*, 2013, **107**, 292-300.

68. H.-Y. Lee, W. Vogel and P. P.-J. Chu, *Langmuir*, 2011, **27**, 14654-14661.

69. X. Zhang, G. Xia, C. Huang and Y. Wang, *Int. J. Hydrogen Energy*, 2013, **38**, 8909-8913.

70. S. Wang, S. P. Jiang, T. J. White, J. Guo and X. Wang, *J. Phys. Chem. C*, 2009, **113**, 18935-18945.

71. B. Luo, X. Yan, S. Xu and Q. Xue, *Electrochim. Acta*, 2012, **59**, 429-434.

72. J.-D. Qiu, G.-C. Wang, R.-P. Liang, X.-H. Xia and H.-W. Yu, *J. Phys. Chem. C*, 2011, **115**, 15639-15645.

73. J. Y. Park and S. Kim, *Int. J. Hydrogen Energy*, 2013, **38**, 6275-6282.

74. Y. Cheng and S. P. Jiang, *Electrochim. Acta*, 2013, **99**, 124-132.

75. X. Huang, Z. Li, X. Zhang, X. He and S. Lin, *J. Colloid Interface Sci.*, 2013, **393**, 300-305.

76. H. Ismaili, F. Lagugne-Labarthet and M. S. Workentin, *Chem. Mater.*, 2011, **23**, 1519-1525.

77. X. Huang, X. Qi, F. Boey and H. Zhang, *Chem. Soc. Rev.*, 2012, **41**, 666-686.

78. S. Liu, J. Wang, J. Zeng, J. Ou, Z. Li, X. Liu and S. Yang, *J. Power Sources*, 2010, **195**, 4628-4633.

79. Y.-G. Zhou, J.-J. Chen, F.-b. Wang, Z.-H. Sheng and X.-H. Xia, *Chem. Commun.*, 2010, **46**, 5951-5953.

80. C.-T. Hsieh, J.-M. Wei, H.-T. Hsiao and W.-Y. Chen, *Electrochimica Acta*, 2012, **64**, 177-182.

81. S. H. Ahn, I. Choi, O. J. Kwon and J. J. Kim, *Chemical Engineering Journal*, 2012, **181–182**, 276-280.

82. Z. Yao, M. Zhu, F. Jiang, Y. Du, C. Wang and P. Yang, *J. Mater. Chem.* 2012, **22**, 13707-13713.

83. Y. Hu, H. Zhang, P. Wu, H. Zhang, B. Zhou and C. Cai, *Phys. Chem. Chem. Phys.*, 2011, **13**, 4083-4094.

84. S. Cheng, R. E. Rettew, M. Sauerbrey and F. M. Alamgir, *Acs Appl. Mater. Interfaces*, 2011, **3**, 3948-3956.

85. S. Sattayasamitsathit, Y. Gu, K. Kaufmann, W. Jia, X. Xiao, M. Rodriguez, S. Minteer, J. Cha, D. B. Burckel, C. Wang, R. Polsky and J. Wang, *J. Mater. Chem. A*, 2013, **1**, 1639-1645.

86. Q. Shi and S. Mu, *J. Power Sources*, 2012, **203**, 48-56.

87. Z. Yao, R. Yue, C. Zhai, F. Jiang, H. Wang, Y. Du, C. Wang and P. Yang, *Int. J. Hydrogen Energy*, 2013, **38**, 6368-6376.

88. L. Gao, L. Ding and L. Fan, *Electrochim. Acta*, 2013, **106**, 159-164.

89. H. Wang, J. Du, Z. Yao, R. Yue, C. Zhai, F. Jiang, Y. Du, C. Wang and P. Yang, *Colloids Surfaces A*, 2013, **436**, 57-61.

90. F. Gao, N. Yang, W. Smirnov, H. Obloh and C. E. Nebel, *Electrochim. Acta*, 2013, **90**, 445-451.

91. D. Santiago, G. G. Rodríguez-Calero, H. Rivera, D. A. Tryk, M. A. Scibioh and C. R. Cabrera, *J. Electrochem. Soc.*, 2010, **157**, F189-F195.

92. D. Santiago, G. G. Rodríguez-Calero, A. Palkar, D. Barraza-Jimenez, D. H. Galvan, G. Casillas, A. Mayoral, M. Jose-Yacamán, L. Echegoyen and C. R. Cabrera, *Langmuir*, 2012, **28**, 17202-17210.

93. H. C. Choi, M. Shim, S. Bangsaruntip and H. Dai, *J. Am. Chem. Soc.*, 2002, **124**, 9058-9059.

94. X.-W. Liu, J.-J. Mao, P.-D. Liu and X.-W. Wei, *Carbon*, 2011, **49**, 477-483.

95. L. Qu and L. Dai, *J. Am. Chem. Soc.*, 2005, **127**, 10806-10807.

96. L. Gao, W. Yue, S. Tao and L. Fan, *Langmuir*, 2012, **29**, 957-964.

97. Y. A. Goh, X. Chen, F. M. Yasin, P. K. Eggers, R. A. Boulos, X. Wang, H. T. Chua and C. L. Raston, *Chem. Commun.*, 2013, **49**, 5171-5173.

98. Q. Wang, B. Geng and B. Tao, *J. Power Sources*, 2011, **196**, 191-195.

99. N. Shang, P. Papakonstantinou, P. Wang and S. R. P. Silva, *J. Phys. Chem. C*, 2010, **114**, 15837-15841.

100. S. Sun, G. Zhang, N. Gauquelin, N. Chen, J. Zhou, S. Yang, W. Chen, X. Meng, D. Geng, M. N. Banis, R. Li, S. Ye, S. Knights, G. A. Botton, T.-K. Sham and X. Sun, *Sci. Rep.*, 2013, **3**.

101. H.-B.-R. Lee, S. H. Baeck, T. F. Jaramillo and S. F. Bent, *Nano Lett.*, 2013, **13**, 457-463.

102. H.-T. Kim, J.-K. Lee and J. Kim, *J. Power Sources*, 2008, **180**, 191-194.

103. S. Sharma, A. Ganguly, P. Papakonstantinou, X. P. Miao, M. X. Li, J. L. Hutchison, M. Delichatsios and S. Ukleja, *J. Phys. Chem. C*, 2010, **114**, 19459-19466.

104. H. Wang, X. Sun, Y. Ye and S. Qiu, *J. Power Sources*, 2006, **161**, 839-842.

105. A. A. Dameron, T. S. Olson, S. T. Christensen, J. E. Leisch, K. E. Hurst, S. Pylypenko, J. B. Bult, D. S. Ginley, R. P. O'Hayre, H. N. Dinh and T. Gennett, *ACS Catal.*, 2011, **1**, 1307-1315.

106. M. Umeda, K. Nagai, M. Shibamine and M. Inoue, *Phys. Chem. Chem. Phys.*, 2010, **12**, 7041-7049.

107. M. Umeda, Y. Matsumoto, M. Inoue and S. Shironita, *Electrochim. Acta*, 2013, **101**, 142-150.

108. S. Shironita, M. Ueda, Y. Matsumoto and M. Umeda, *J. Power Sources*, 2013, **243**, 635-640.

109. K.-S. Yao, Y.-C. Chen, C.-H. Chao, W.-F. Wang, S.-Y. Lien, H. C. Shih, T.-L. Chen and K.-W. Weng, *Thin Solid Films*, 2010, **518**, 7225-7228.

110. A. R. Corpuz, T. S. Olson, P. Joghee, S. Pylypenko, A. A. Dameron, H. N. Dinh, K. J. O'Neill, K. E. Hurst, G. Bender, T. Gennett, B. S. Pivovar, R. M. Richards and R. P. O'Hayre, *J. Power Sources*, 2012, **217**, 142-151.

111. K. Hirakawa, M. Inoue and T. Abe, *Electrochim. Acta*, 2010, **55**, 5874-5880.

112. C. Zhang, J. Hu, M. Nagatsu, X. Shu, H. Toyoda, S. Fang and Y. Meng, *Electrochim. Acta*, 2011, **56**, 6033-6040.

113. K. Yoshii, T. Tsuda, T. Arimura, A. Imanishi, T. Torimoto and S. Kuwabata, *RSC Advances*, 2012, **2**, 8262-8264.

114. V. Matolín, I. Matolínová, M. Václavu□, I. Khalakhan, M. Vorokhta, R. Fiala, I. Pis□, Z. Sofer, J. Poltierová-Vejpravová, T. Mori, V. Potin, H. Yoshikawa, S. Ueda and K. Kobayashi, *Langmuir*, 2010, **26**, 12824-12831.

115. C.-Y. Su, Y.-C. Hsueh, C.-C. Kei, C.-T. Lin and T.-P. Perng, *J. Phys. Chem. C*, 2013, **117**, 11610-11618.

116. Y. Chen, J. Wang, X. Meng, Y. Zhong, R. Li, X. Sun, S. Ye and S. Knights, *Int. J. Hydrogen Energy*, 2011, **36**, 11085-11092.

117. A. Tabet-Aoul and M. Mohamedi, *Phys. Chem. Chem. Phys.*, 2012, **14**, 4463-4474.

118. X. Ma, L. Luo, L. Zhu, L. Yu, L. Sheng, K. An, Y. Ando and X. Zhao, *J. Power Sources*, 2013, **241**, 274-280.

119. P. Kundu, C. Nethravathi, P. A. Deshpande, M. Rajamathi, G. Madras and N. Ravishankar, *Chem. Mater.*, 2011, **23**, 2772-2780.

120. C.-T. Hsieh, W.-Y. Chen, I. L. Chen and A. K. Roy, *J. Power Sources*, 2012, **199**, 94-102.

121. R. Lu, J. B. Zang, Y. H. Wang and Y. L. Zhao, *Electrochim. Acta*, 2012, **60**, 329-333.

122. C.-T. Hsieh, W.-M. Hung, W.-Y. Chen and J.-Y. Lin, *Int. J. Hydrogen Energy*, 2011, **36**, 2765-2772.

123. Y. Zhang, G. Chang, S. Liu, J. Tian, L. Wang, W. Lu, X. Qin and X. Sun, *Catal. Sci. Technol.*, 2011, **1**, 1636-1640.

124. C.-S. Liao, C.-T. Liao, C.-Y. Tso and H.-J. Shy, *Mater. Chem. Phys.*, 2011, **130**, 270-274.

125. K. M. Samant, V. S. Joshi, G. Sharma, S. Kapoor and S. K. Haram, *Electrochim. Acta*, 2011, **56**, 2081-2086.

126. H. Li, G. Chang, Y. Zhang, J. Tian, S. Liu, Y. Luo, A. M. Asiri, A. O. Al-Youbi and X. Sun, *Catal. Sci. Technol.*, 2012, **2**, 1153-1156.

127. J. N. Tiwari, R. N. Tiwari, G. Singh and K. S. Kim, *Nano Energy*, 2013, **2**, 553-578.

128. E. Antolini, *Appl. Catal. B*, 2009, **88**, 1-24.

129. Y. Liu, C. Ji, W. Gu, J. Jorne and H. A. Gasteiger, *J. Electrochem. Soc.*, 2011, **158**, B614-B621.

130. A. D. Moore, S. M. Holmes and E. P. L. Roberts, *RSC Advances*, 2012, **2**, 1669-1674.

131. W.-L. Qu, Z.-B. Wang, Z.-Z. Jiang, D.-M. Gu and G.-P. Yin, *RSC Advances*, 2012, **2**, 344-350.

132. C. Alegre, M. E. Gálvez, E. Baquedano, R. Moliner, E. Pastor and M. J. Lázaro, *J. Phys. Chem. C*, 2013, **117**, 13045-13058.

133. J. R. C. Salgado, V. A. Paganin, E. R. Gonzalez, M. F. Montemor, I. Tacchini, A. Ansón, M. A. Salvador, P. Ferreira, F. M. L. Figueiredo and M. G. S. Ferreira, *Int. J. Hydrogen Energy*, 2013, **38**, 910-920.

134. Q. Jiang, L. Jiang, H. Hou, J. Qi, S. Wang and G. Sun, *J. Phys. Chem. C*, 2010, **114**, 19714-19722.

135. C.-W. Kuo, I. T. Lu, L.-C. Chang, Y.-C. Hsieh, Y.-C. Tseng, P.-W. Wu and J.-F. Lee, *J.Power Sources*, 2013, **240**, 122-130.

136. J. Zeng, *J. Mater. Chem.*, 2012, **22**, 3170-3176.

137. O. Sahin and H. Kivrak, *Int. J. Hydrogen Energy*, 2013, **38**, 901-909.

138. J. Qi, L. Jiang, Q. Tang, S. Zhu, S. Wang, B. Yi and G. Sun, *Carbon*, 2012, **50**, 2824-2831.

139. F. Su, C. K. Poh, Z. Tian, G. Xu, G. Koh, Z. Wang, Z. Liu and J. Lin, *Energy Fuels*, 2010, **24**, 3727-3732.

140. T. Maiyalagan, T. O. Alaje and K. Scott, *J. Phys. Chem. C*, 2011, **116**, 2630-2638.

141. L. Calvillo, V. Celorrio, R. Moliner, A. B. Garcia, I. Caméan and M. J. Lazaro, *Electrochim. Acta*, 2013, **102**, 19-27.

142. Z.-B. Wang, C.-R. Zhao, P.-F. Shi, Y.-S. Yang, Z.-B. Yu, W.-K. Wang and G.-P. Yin, *J. Phys. Chem. C*, 2009, **114**, 672-677.

143. J. Cao, Z. Chen, J. Xu, W. Wang and Z. Chen, *Electrochim. Acta*, 2013, **88**, 184-192.

144. S.-J. Park, B.-J. Kim and S.-Y. Lee, *J. Colloid Interface Sci.*, 2013, **405**, 150-156.

145. S. Kang, S. Lim, D.-H. Peck, S.-K. Kim, D.-H. Jung, S.-H. Hong, H.-G. Jung and Y. Shul, *Int. J. Hydrogen Energy*, 2012, **37**, 4685-4693.

146. A. Santasalo-Aarnio, M. Borghei, I. V. Anoshkin, A. G. Nasibulin, E. I. Kauppinen, V. Ruiz and T. Kallio, *Int. J. Hydrogen Energy*, 2012, **37**, 3415-3424.

147. C. A. Bessel, K. Laubernds, N. M. Rodriguez and R. T. K. Baker, *J. Phys. Chem. B*, 2001, **105**, 1115-1118.

148. E. S. Steigerwalt, G. A. Deluga and C. M. Lukehart, *J. Phys. Chem. B*, 2002, **106**, 760-766.

149. P. Serp, M. Corrias and P. Kalck, *Appl. Catal. A*, 2003, **253**, 337-358.

150. B. Singh and E. Dempsey, *RSC Advances*, 2013, **3**, 2279-2287.

151. R. H. Baughman, A. A. Zakhidov and W. A. de Heer, *Science*, 2002, **297**, 787-792.

152. M. F. L. De Volder, S. H. Tawfick, R. H. Baughman and A. J. Hart, *Science*, 2013, **339**, 535-539.

153. G. Girishkumar, K. Vinodgopal and P. V. Kamat, *J. Phys. Chem. B*, 2004, **108**, 19960-19966.

154. G. Girishkumar, T. D. Hall, K. Vinodgopal and P. V. Kamat, *J. Phys. Chem. B*, 2006, **110**, 107-114.

155. R. Chetty, W. Xia, S. Kundu, M. Bron, T. Reinecke, W. Schuhmann and M. Muhler, *Langmuir*, 2009, **25**, 3853-3860.

156. D. Mirabile Gattia, M. V. Antisari, L. Giorgi, R. Marazzi, E. Piscopiello, A. Montone, S. Bellitto, S. Licoccia and E. Traversa, *J. Power Sources*, 2009, **194**, 243-251.

157. W. Tokarz, G. Lota, E. Frackowiak, A. Czerwiński and P. Piela, *Electrochim. Acta*, 2013, **98**, 94-103.

158. H. Jiang, T. Zhao, C. Li and J. Ma, *Chem. Commun.*, 2011, **47**, 8590-8592.

159. H. Huang, D. Sun and X. Wang, *J. Phys. Chem. C*, 2011, **115**, 19405-19412.

160. Q.-L. Naidoo, S. Naidoo, L. Petrik, A. Nechaev and P. Ndungu, *Int. J. Hydrogen Energy*, 2012, **37**, 9459-9469.

161. N. Kakati, J. Maiti, S. H. Lee and Y. S. Yoon, *Int. J. Hydrogen Energy*, 2012, **37**, 19055-19064.

162. H. Huang, Y. Fan and X. Wang, *Electrochim. Acta*, 2012, **80**, 118-125.

163. Y. Huang, J. Cai, S. Zheng and Y. Guo, *J. Power Sources*, 2012, **210**, 81-85.

164. J. Yuan, B. He, L. Hong, J. Lu, J. Miao and L. Niu, *J. Mater. Chem.*, 2012, **22**, 19658-19665.

165. K. S. Novoselov, A. K. Geim, S. V. Morozov, D. Jiang, Y. Zhang, S. V. Dubonos, I. V. Grigorieva and A. A. Firsov, *Science*, 2004, **306**, 666-669.

166. S. Stankovich, D. A. Dikin, G. H. B. Dommett, K. M. Kohlhaas, E. J. Zimney, E. A. Stach, R. D. Piner, S. T. Nguyen and R. S. Ruoff, *Nature*, 2006, **442**, 282-286.

167. D. Li and R. B. Kaner, *Science*, 2008, **320**, 1170-1171.

168. V. Singh, D. Joung, L. Zhai, S. Das, S. I. Khondaker and S. Seal, *Prog. Mater. Sci.*, 2011, **56**, 1178-1271.

169. A. K. Geim and K. S. Novoselov, *Nat. Mater.*, 2007, **6**, 183-191.

170. C. N. R. Rao, A. K. Sood, K. S. Subrahmanyam and A. Govindaraj, *Angew. Chem. Int. Ed.*, 2009, **48**, 7752-7777.

171. Y. Sun, Q. Wu and G. Shi, *Energy Environ. Sci.*, 2011, **4**, 1113-1132.

172. C. Huang, C. Li and G. Shi, *Energy Environ. Sci.*, 2012, **5**, 8848-8868.

173. Y. M. Li, L. H. Tang and J. H. Li, *Electrochem. Commun.*, 2009, **11**, 846-849.

174. Y. J. Li, W. Gao, L. J. Ci, C. M. Wang and P. M. Ajayan, *Carbon*, 2010, **48**, 1124-1130.

175. S. Bong, Y.-R. Kim, I. Kim, S. Woo, S. Uhm, J. Lee and H. Kim, *Electrochem. Commun.*, 2010, **12**, 129-131.

176. K. Ji, G. Chang, M. Oyama, X. Shang, X. Liu and Y. He, *Electrochim. Acta*, 2012, **85**, 84-89.

177. T. Tomai, Y. Kawaguchi, S. Mitani and I. Honma, *Electrochim. Acta*, 2013, **92**, 421-426.

178. J. Zhao, L. Zhang, T. Chen, H. Yu, L. Zhang, H. Xue and H. Hu, *J. Phys. Chem. C*, 2012, **116**, 21374-21381.

179. L. F. Dong, R. R. S. Gari, Z. Li, M. M. Craig and S. F. Hou, *Carbon*, 2010, **48**, 781-787.

180. S. H. Lee, N. Kakati, S. H. Jee, J. Maiti and Y.-S. Yoon, *Mater. Lett.*, 2011, **65**, 3281-3284.

181. J. Zhao, L. Zhang, H. Xue, Z. Wang and H. Hu, *RSC Advances*, 2012, **2**, 9651-9659.

182. H. Zhang, X. Xu, P. Gu, C. Li, P. Wu and C. Cai, *Electrochim. Acta*, 2011, **56**, 7064-7070.

183. Y. Lu, Y. Jiang, H. Wu and W. Chen, *J. Phys. Chem. C*, 2013, **117**, 2926-2938.

184. H. Huang, D. Sun and X. Wang, *Chin. Sci. Bull.*, 2012, **57**, 3071-3079.

185. J. Shen, B. Yan, M. Shi, H. Ma, N. Li and M. Ye, *Mater. Res. Bull.*, 2012, **47**, 1486-1493.

186. B. Luo, X. Yan, J. Chen, S. Xu and Q. Xue, *Int. J. Hydrogen Energy*, 2013, **38**, 13011-13016.

187. Z. Ji, G. Zhu, X. Shen, H. Zhou, C. Wu and M. Wang, *New J. Chem.*, 2012, **36**, 1774-1780.

188. H. Mao, R. Li, K. Jiang, T. Huang and A. Yu, *Electrochim. Acta*, 2013, **107**, 419-424.

189. F. Han, X. Wang, J. Lian and Y. Wang, *Carbon*, 2012, **50**, 5498-5504.

190. R. Awasthi and R. N. Singh, *Carbon*, 2013, **51**, 282-289.

191. M. Zhang, Z. Yan, Q. Sun, J. Xie and J. Jing, *New J. Chem.*, 2012, **36**, 2533-2540.

192. Y. Zhang, Y.-e. Gu, S. Lin, J. Wei, Z. Wang, C. Wang, Y. Du and W. Ye, *Electrochim. Acta*, 2011, **56**, 8746-8751.

193. S. M. Choi, M. H. Seo, H. J. Kim and W. B. Kim, *Carbon*, 2011, **49**, 904-909.

194. Y. Liu, Y. Huang, Y. Xie, Z. Yang, H. Huang and Q. Zhou, *Chem. Eng. J.*, 2012, **197**, 80-87.

195. C. Nethravathi, E. A. Anumol, M. Rajamathi and N. Ravishankar, *Nanoscale*, 2011, **3**, 569-571.

196. H. Huang and X. Wang, *J.Mater. Chem.*, 2012, **22**, 22533-22541.

197. T. Maiyalagan, X. Dong, P. Chen and X. Wang, *J. Mater. Chem.*, 2012, **22**, 5286-5290.

198. H. Qiu, X. Dong, B. Sana, T. Peng, D. Paramelle, P. Chen and S. Lim, *Acs Appl. Mater. Interfaces*, 2013, **5**, 782-787.

199. S. Wei, D. Wu, X. Shang and R. Fu, *Energy Fuels*, 2009, **23**, 908-911.

200. M. Khosravi and M. K. Amini, *Int. J. Hydrogen Energy*, 2010, **35**, 10527-10538.

201. Y. Zhang, L. Jiang, H. Li, L. Fan, W. Hu, C. Wang, Y. Li and S. Yang, *Chem. -Eur. J.*, 2011, **17**, 4921-4926.

202. T. Bordjiba, M. Mohamedi, L. H. Dao, B. Aissa and M. A. El Khakani, *Chem. Phys. Lett.*, 2007, **441**, 88-93.

203. Y. M. Chang, Y. C. Hsieh and P. W. Wu, *Diam. Relat. Mater.*, 2009, **18**, 501-504.

204. M. Kosaka, S. Kuroshima, K. Kobayashi, S. Sekino, T. Ichihashi, S. Nakamura, T. Yoshitake and Y. Kubo, *J. Phys. Chem. C*, 2009, **113**, 8660-8667.

205. W.-F. Chen, J.-P. Wang, C.-H. Hsu, J.-Y. Jhan, H. Teng and P.-L. Kuo, *J. Phys. Chem. C*, 2010, **114**, 6976-6982.

206. C.-T. Hsieh, W.-M. Hung and W.-Y. Chen, *Int. J. Hydrogen Energy*, 2010, **35**, 8425-8432.

207. C.-H. Wang, H.-Y. Du, H.-C. Hsu, S.-T. Chang, H.-C. Huang, L.-C. Chen and K.-H. Chen, *Int. J. Hydrogen Energy*, 2012, **37**, 10663-10670.

208. Y. Chang, G. Han, M. Li and F. Gao, *Carbon*, 2011, **49**, 5158-5165.

209. X. Bo and L. Guo, *Electrochim. Acta*, 2013, **90**, 283-290.

210. S.-Y. Yang, K.-H. Chang, Y.-F. Lee, C.-C. M. Ma and C.-C. Hu, *Electrochem. Commun.*, 2010, **12**, 1206-1209.

211. Y.-S. Wang, S.-Y. Yang, S.-M. Li, H.-W. Tien, S.-T. Hsiao, W.-H. Liao, C.-H. Liu, K.-H. Chang, C.-C. M. Ma and C.-C. Hu, *Electrochim. Acta*, 2013, **87**, 261-269.

212. N. Jha, R. I. Jafri, N. Rajalakshmi and S. Ramaprabhu, *Int. J. Hydrogen Energy*, 2011, **36**, 7284-7290.

213. R. Lv, T. Cui, M.-S. Jun, Q. Zhang, A. Cao, D. S. Su, Z. Zhang, S.-H. Yoon, J. Miyawaki, I. Mochida and F. Kang, *Adv. Funct. Mater.*, 2011, **21**, 999-1006.

214. J.-Y. Jhan, Y.-W. Huang, C.-H. Hsu, H. Teng, D. Kuo and P.-L. Kuo, *Energy*, 2013, **53**, 282-287.

215. H. Wang, T. Maiyalagan and X. Wang, *ACS Catal.*, 2012, **2**, 781-794.

216. D. Wei, Y. Liu, Y. Wang, H. Zhang, L. Huang and G. Yu, *Nano Lett.*, 2009, **9**, 1752-1758.

217. L. S. Panchakarla, K. S. Subrahmanyam, S. K. Saha, A. Govindaraj, H. R. Krishnamurthy, U. V. Waghmare and C. N. R. Rao, *Adv. Mater.*, 2009, **21**, 4726-4730.

218. Y. Shao, J. Sui, G. Yin and Y. Gao, *Appl. Catal. B*, 2008, **79**, 89-99.

219. B. Xiong, Y. Zhou, Y. Zhao, J. Wang, X. Chen, R. O'Hayre and Z. Shao, *Carbon*, 2013, **52**, 181-192.

220. G. Yang, Y. Li, R. K. Rana and J.-J. Zhu, *J. Mater. Chem. A*, 2013, **1**, 1754-1762.

221. Y.-H. Li, T.-H. Hung and C.-W. Chen, *Carbon*, 2009, **47**, 850-855.

222. Y. Wang, Y. Shao, D. W. Matson, J. Li and Y. Lin, *Acs Nano*, 2010, **4**, 1790-1798.

223. Y. Zhou, K. Neyerlin, T. S. Olson, S. Pylypenko, J. Bult, H. N. Dinh, T. Gennett, Z. Shao and R. O'Hayre, *Energ Environ. Sci.*, 2010, **3**, 1437-1446.

224. F. Su, Z. Tian, C. K. Poh, Z. Wang, S. H. Lim, Z. Liu and J. Lin, *Chem. Mater.*, 2009, **22**, 832-839.

225. C. Pan, L. Qiu, Y. Peng and F. Yan, *J. Mater. Chem.*, 2012, **22**, 13578-13584.

226. P.-L. Kuo and C.-H. Hsu, *Acs Appl. Mater. Interfaces*, 2010, **3**, 115-118.

227. C.-H. Hsu and P.-L. Kuo, *J. Power Sources*, 2012, **198**, 83-89.

228. D. Geng, Y. Hu, Y. Li, R. Li and X. Sun, *Electrochem. Commun.*, 2012, **22**, 65-68.
229. C.-H. Hsu, H.-M. Wu and P.-L. Kuo, *Chem. Commun.*, 2010, **46**, 7628-7630.
5 230. Z. Liu, F. Su, X. Zhang and S. W. Tay, *Acs Appl. Mater. Interfaces*, 2011, **3**, 3824-3830.
231. L.-S. Zhang, X.-Q. Liang, W.-G. Song and Z.-Y. Wu, *Phys. Chem. Chem. Phys.*, 2010, **12**, 12055-12059.
232. Y. Xin, J.-g. Liu, X. Jie, W. Liu, F. Liu, Y. Yin, J. Gu and Z. Zou,
10 *Electrochim. Acta*, 2012, **60**, 354-358.
233. S. Pylypenko, A. Borisevich, K. L. More, A. R. Corpuz, T. Holme, A. A. Dameron, T. S. Olson, H. N. Dinh, T. Gennett and R. O'Hayre, *Energy Environ. Sci.*, 2013, **6**, 2957-2964.
234. S. Wang, T. Cochell and A. Manthiram, *Phys. Chem. Chem. Phys.*,
15 2012, **14**, 13910-13913.
235. L. La-Torre-Riveros, R. Guzman-Blas, A. E. Méndez-Torres, M. Prelas, D. A. Tryk and C. R. Cabrera, *Acs Appl. Mater. Interfaces*, 2012, **4**, 1134-1147.
236. R. Ahmadi and M. K. Amini, *Int. J. Hydrogen Energy*, 2011, **36**,
20 7275-7283.
237. R. Ahmadi, M. K. Amini and J. C. Bennett, *J.Catal.*, 2012, **292**, 81-89.
238. S. Sun, G. Zhang, D. Geng, Y. Chen, M. N. Banis, R. Li, M. Cai and X. Sun, *Chem.–Eur. J.*, 2010, **16**, 829-835.
25 239. H. Song, X. Qiu, D. Guo and F. Li, *J. Power Sources*, 2008, **178**, 97-102.
240. Z. Chen, X. Qiu, B. Lu, S. Zhang, W. Zhu and L. Chen, *Electrochem. Commun.*, 2005, **7**, 593-596.
241. E. Lee and A. Manthiram, *J. Phys. Chem. C*, 2010, **114**, 21833-
30 21839.
242. C. Feng, T. Takeuchi, M. A. Abdelkareem, T. Tsujiguchi and N. Nakagawa, *J. Power Sources*, 2013, **242**, 57-64.
243. S. Yu, Q. Liu, W. Yang, K. Han, Z. Wang and H. Zhu, *Electrochim. Acta*, 2013, **94**, 245-251.
35 244. Y.-Y. Chu, Z.-B. Wang, Z.-Z. Jiang, D.-M. Gu and G.-P. Yin, *Adv. Mater.*, 2011, **23**, 3100-3104.
245. X. Wang, X. Li, D. Liu, S. Song and H. Zhang, *Chem. Commun.*, 2012, **48**, 2885-2887.
246. S. K. Meher and G. R. Rao, *ACS Catal.*, 2012, **2**, 2795-2809.
40 247. Z. Sun, X. Wang, Z. Liu, H. Zhang, P. Yu and L. Mao, *Langmuir*, 2010, **26**, 12383-12389.
248. D. R. Ou, T. Mori, H. Togasaki, M. Takahashi, F. Ye and J. Drennan, *Langmuir*, 2011, **27**, 3859-3866.
249. S. Chen, J. Zhu, X. Wu, Q. Han and X. Wang, *ACS Nano*, 2010, **4**,
45 2822-2830.
250. H. Huang and X. Wang, *Nanoscale*, 2011, **3**, 3185-3191.
251. C. Zhou, H. Wang, F. Peng, J. Liang, H. Yu and J. Yang, *Langmuir*, 2009, **25**, 7711-7717.
252. C. Zhou, F. Peng, H. Wang, H. Yu, C. Peng and J. Yang,
50 *Electrochem. Commun.*, 2010, **12**, 1210-1213.
253. Y. Zhao, L. Zhan, J. Tian, S. Nie and Z. Ning, *Int. J. Hydrogen Energy*, 2010, **35**, 10522-10526.
254. R. Liu, H. Zhou, J. Liu, Y. Yao, Z. Huang, C. Fu and Y. Kuang, *Electrochem.Commun.*, 2013, **26**, 63-66.
55 255. H. Huang, Q. Chen, M. He, X. Sun and X. Wang, *J. Power Sources*, 2013, **239**, 189-195.
256. H. Huang and X. Wang, *Phys. Chem. Chem. Phys.*, 2013, **15**, 10367-10375.
257. S. Devaraj and N. Munichandraiah, *J. Phys. Chem. C*, 2008, **112**,
60 4406-4417.
258. S. Chen, J. Zhu, Q. Han, Z. Zheng, Y. Yang and X. Wang, *Cryst. Growth Des.*, 2009, **9**, 4356-4361.
259. L. Yang, Y. Xiao, G. Zeng, S. Luo, S. Kuang and Q. Cai, *Energy Fuels*, 2009, **23**, 3134-3138.
65 260. T. Saida, N. Ogiwara, Y. Takasu and W. Sugimoto, *J. Phys. Chem. C*, 2010, **114**, 13390-13396.
261. B. Y. Xia, H. B. Wu, J. S. Chen, Z. Wang, X. Wang and X. W. Lou, *Phys. Chem. Chem. Phys.*, 2012, **14**, 473-476.
262. H. He, P. Xiao, M. Zhou, F. Liu, S. Yu, L. Qiao and Y. Zhang,
70 *Electrochim. Acta*, 2013, **88**, 782-789.

263. M. Hepel, I. Kumarihamy and C. J. Zhong, *Electrochem. Commun.*, 2006, **8**, 1439-1444.
264. Y. Ito, T. Takeuchi, T. Tsujiguchi, M. A. Abdelkareem and N. Nakagawa, *J. Power Sources*, 2013, **242**, 280-288.
75 265. B. Y. Xia, B. Wang, H. B. Wu, Z. Liu, X. Wang and X. W. Lou, *J. Mater. Chem.*, 2012, **22**, 16499-16505.
266. Y. Fan, Z. Yang, P. Huang, X. Zhang and Y.-M. Liu, *Electrochim. Acta*, 2013, **105**, 157-161.
267. Y.-L. Shen, S.-Y. Chen, J.-M. Song and I.-G. Chen, *Nanoscale Res.*
80 *Lett.*, 2012, **7**, 1-5.
268. P. Justin and G. Ranga Rao, *Int. J. Hydrogen Energy*, 2011, **36**, 5875-5884.
269. R. S. Amin, R. M. Abdel Hameed, K. M. El-Khatib, H. El-Abd and E. R. Souaya, *Int. J. Hydrogen Energy*, 2012, **37**, 18870-18881.
85 270. X. Yang, X. Wang, G. Zhang, J. Zheng, T. Wang, X. Liu, C. Shu, L. Jiang and C. Wang, *Int. J. Hydrogen Energy*, 2012, **37**, 11167-11175.
271. K.-H. Ye, S.-A. Zhou, X.-C. Zhu, C.-W. Xu and P. K. Shen, *Electrochim. Acta*, 2013, **90**, 108-111.
272. J. Zeng, C. Francia, C. Gerbaldi, V. Baglio, S. Specchia, A. S. Aricò
90 and P. Spinelli, *Electrochim. Acta*, 2013, **94**, 80-91.
273. B. K. Balan and S. Kurungot, *Inorg. Chem.*, 2012, **51**, 9766-9774.
274. N. Kakati, J. Maiti, S. H. Jee, S. H. Lee and Y. S. Yoon, *J. Alloys Compd.*, 2011, **509**, 5617-5622.
275. P. Justin, P. Hari Krishna Charan and G. Ranga Rao, *Appl. Catal. B*,
95 2010, **100**, 510-515.
276. Y.-J. Wang, D. P. Wilkinson and J. Zhang, *Chem. Rev.*, 2011, **111**, 7625-7651.
277. X. Yuan, X.-L. Ding, C.-Y. Wang and Z.-F. Ma, *Energy Environ. Sci.*, 2013, **6**, 1105-1124.
100 278. H. Gao, J.-B. He, Y. Wang and N. Deng, *J. Power Sources*, 2012, **205**, 164-172.
279. Z. Cui, C. M. Li and S. P. Jiang, *Phys. Chem. Chem. Phys.*, 2011, **13**, 16349-16357.
280. A. Siriviriyanun and T. Imae, *Phys. Chem. Chem. Phys.*, 2013, **15**,
105 4921-4929.

Table of contents graphic
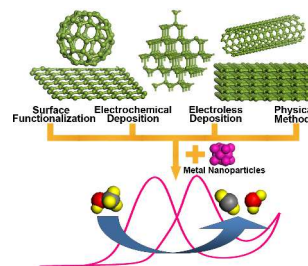
This review summarizes recent significant progress in the
110 fabrication and applications of carbon-based anode catalysts for direct methanol fuel cells.

115

120

125

5

10

Biographies

Professor Xin Wang received his PhD degree under the supervision of Professor Anbang Dai and Professor Xinquan Xin at Nanjing University in 1985. After that, he joined Nanjing University of Science and Technology and was promoted to full professor in 1988. His research interests are focused on synthesizing nanostructured materials for use in catalytic and energy storage applications. He received two second-place prizes of the State Science and Technology Progress Award (China) in 2005 and 2010, respectively.

30

Huajie Huang received the Bachelor's degree in material chemistry from Nanjing University of Science and Technology in 2009. Currently he is a PhD candidate under the supervision of Professor Xin Wang at the same university. From December, 2012 to December, 2013, he joined Professor Pulickel M. Ajayan's group at Rice University as an exchange visiting scholar. His research interests focus on synthesis of carbon-based nanocomposites for energy conversion and storage applications.